Dyakonov-Shur instability of the electronic fluid: Spectral effect of weak magnetic field

Matthias Maier [1,*] Dennis Corraliza-Rodriguez [2,†] and Dionisios Margetis [3,‡]

[1] *Department of Mathematics, Texas A&M University, College Station, Texas 77843, USA*

[2] *Center for Applied Mathematics, Cornell University, Ithaca, New York 14853, USA*

[3] *Institute for Physical Science and Technology, and Department of Mathematics, University of Maryland, College Park, Maryland 20742, USA*

(Received 22 March 2024; revised 5 September 2024; accepted 23 September 2024; published 15 October 2024)

We study numerically and analytically how the Dyakonov-Shur instability for a two-dimensional (2D) inviscid electronic fluid in a long channel can be affected by an external, out-of-plane static magnetic field. By linear stability analysis for a model based on the shallow-water equations, we describe the discrete spectrum of frequencies. When the fluid system is near the subsonic-to-supersonic transition point, a magnetically controlled gap between the stability and instability spectra of the complex eigenfrequencies is evident by our computations. This suggests that, within this model, the passage from stability to instability (and vice versa) is no longer continuous in the effective Mach parameter of the boundary conditions. We also demonstrate that the growth exponents are enhanced by the magnetic field. In a regime of weak magnetic fields, we derive a scaling law for the eigenfrequencies by perturbation theory. We discuss theoretical implications of our results in efforts to generate terahertz electromagnetic radiation by 2D electronic transport.

DOI: 10.1103/PhysRevB.110.165132

I. INTRODUCTION

For the last two decades, the problem of efficiently generating electromagnetic radiation at terahertz (THz) frequencies has received considerable attention [1–6]. Research in this direction is motivated by a plethora of potential applications, which include the identification of distinct chemical processes, diagnostics for industrial and environmental purposes, biomedical sensing and imaging, and the monitoring of microscopic dynamics in semiconductors and nanomaterials [2]. THz waves are technologically appealing since they may attenuate slowly with wavelengths suitable for nanoscale sensing [7–9]. Experimental designs for the generation of THz waves aim to capture motions of microscale dynamics, e.g., vibrations of large molecules and electronic transitions [10–12].

At the same time, there are intensive efforts to harness properties of two-dimensional (2D) materials such as graphene and van der Waals heterostructures [13–16]. When the size of the sample is large compared to the mean free path for momentum-conserving electron-electron scattering but small compared to the mean free path of momentum-relaxing collisions, the electron system may behave as a fluid [17,18]. This behavior has been observed experimentally; see, e.g., [19–22]. Accordingly, the electronic density and velocity fields can be described by hydrodynamic approaches [18].

Three decades ago, in a seminal paper Dyakonov and Shur (DS) formulated a one-dimensional (1D) model based on the shallow-water equations in their proposal for plasma wave generation in a field effect transistor [23]. A key ingredient of their model is its boundary conditions with fixed electronic surface density and normal flux at the edges of a long channel. By linear stability analysis, this model leads to the prediction of an instability in the subsonic regime [23]; and has inspired the attractive idea of generating THz waves via unstable 2D electronic transport [18]. In the DS theory, the passage from fluid stability to instability can occur by a continuously varying Mach number formed by the intrinsic sound speed and a parameter from the boundary conditions.

To our knowledge, the realization of the DS instability in the laboratory setting remains an alluring yet challenging and elusive goal to date [24,25]. Research efforts to achieve this goal have improved our understanding of how THz charge density waves can be excited and sustained in 2D channels [26–29]. Furthermore, various extensions of the DS model have incorporated more realistic effects such as nonlocality [30], imperfection of the boundaries at the ballistic-to-hydrodynamic crossover [31], and nonlinear effects [24,32]. In principle, the DS instability can be significantly affected by details of the boundary conditions at the crossover regime [31]. In the hydrodynamic limit, the character of this instability is undistorted. The related growth exponents, however, are expected to be reduced by viscous dissipation [18].

In this paper, we study an extension of the DS model by including an external, out-of-plane static magnetic field $\boldsymbol{B}$ in the Lorentz force. The DS boundary conditions for the density and normal flux are left unchanged. We also investigate two distinct choices of the boundary condition for the tangential flux, for comparison purposes. The magnetic field

*Contact author: maier@tamu.edu; https://people.tamu.edu/~maier

†Contact author: dc858@cornell.edu; https://www.cam.cornell.edu/research/grad-students/dennis-corraliza

‡Contact author: diom@umd.edu; https://www.math.umd.edu/~diom

breaks the time-reversal symmetry of the shallow-water equations formulated by DS [23]. By linear stability analysis, we demonstrate how the resulting spectrum differs from the one predicted by DS. Notably, the discrete eigenfrequencies of the requisite non-Hermitian problem no longer lie along a straight line in the complex plane. Near the subsonic-to-supersonic transition point, the complex point spectrum exhibits a *gap* between the imaginary parts of the eigenfrequencies in the stability and instability regimes. Such a gap exists for each of our choices of the boundary condition involving the tangential flux. This finding suggests that it would be theoretically impossible to continuously connect these two regimes by varying the Mach number of the DS model, if the electronic system could be driven in these regimes. A major underlying assumption is the validity of the shallow-water equations of our model. For a weak magnetic field, we describe how the predicted gap scales with $|\boldsymbol{B}|$. Our analysis yields the exact 2D electronic steady state, which in principle depends on the prescribed boundary conditions, via the solution of a nonlinear equation. We discuss implications of our results in efforts to produce THz radiation.

Our paper focuses on exposing generic features of a particular model, based on the Euler equations, for the hydrodynamic regime of 2D electronic systems. We show how a small perturbation of the DS model [23], by use of an external static magnetic field $\boldsymbol{B}$ can cause qualitatively significant changes to related predictions. For fixed nonzero $\boldsymbol{B}$, the electronic steady state is characterized by spatially varying density and flux profiles, in contrast to the constant density and flux in [23]. This steady state is locked into one of two different branches depending on the kinetic regime, or Mach number, of the unperturbed DS model. Fluctuations of the fluid variables around the steady state are bound to a particular branch; and exhibit a stability or instability spectrum. By our numerics, we identify a magnetically controlled, complex-valued spectral gap, in the sense defined below (Sec. V), near the transition point. This gap is related to the multivalued function of the steady-state solution.

It is worthwhile to pose the following question: Can our analysis be useful for future efforts to realize instabilities of 2D electronic fluids, or is it merely an academic exercise? We tend to adopt the former point of view here. We believe that our results offer a cautionary paradigm for modeling electron hydrodynamics, since they suggest how a magnetic perturbation of the DS model [23] can lead to modified predictions such as enhanced growth exponents and a gapped complex-valued spectrum, which might challenge physical interpretation. We attribute this difficulty to the nature of the underlying hydrodynamic model and its boundary conditions. In particular, we discuss how the boundary condition for the tangential flux affects the steady state and the fluid spectrum. The issue of whether the DS instability is experimentally feasible or not is left unresolved. We indicate ranges of values of physical parameters that a 2D system may have to be a plausible testbed for our predictions. However, we are unable to propose a specific material for this purpose.

From a purely theoretical perspective, we investigate a mechanism of time-reversal symmetry breaking of the unperturbed homogeneous system of equations used by DS [23]. To our knowledge, this extension of the DS model has not been previously explored, and paves the way to the study of a broad family of effective hydrodynamic theories lacking basic symmetries. From an applied perspective, we show that the nonzero magnetic field $\boldsymbol{B}$ can plausibly enhance the growth exponents.

Our linear stability analysis largely relies on numerical computations. Technically speaking, in our approach we discretize the differential operator of the requisite non-Hermitian eigenvalue problem for the frequencies by a finite difference approximation scheme. This method enables us to numerically solve the differential equations for the electronic surface density and flux. We compute a large number of the (discrete) complex eigenfrequencies in the fluid stability and instability regimes, and observe their behavior as a function of the $\boldsymbol{B}$ field and the Mach number of the DS model. The $\boldsymbol{B}$ field induces curvature to the continuous curves that interpolate the computed eigenfrequencies. This situation should be contrasted to the case with $\boldsymbol{B} = 0$ of the DS model, when the respective eigenfrequencies lie in straight lines. By our numerics, we notice that as $|\boldsymbol{B}|$ increases, the instability spectrum is shifted towards higher growth for fixed Mach number.

The remainder of this paper is summarized as follows. Section II provides a review of the DS model. We describe the geometry, equations of motion, and boundary conditions (Sec. II A); outline the result of the linear stability analysis (Sec. II B); discuss the sense in which the fluid stability and instability spectra are connected (Sec. II C); and point out a scaling limit (Sec. II D). In Sec. III, we describe the hydrodynamic model with an out-of-plane static magnetic field, $\boldsymbol{B}$: We rescale and nondimensionalize the governing equations (Sec. III A); and derive the electronic steady state via solving an algebraic equation for two distinct choices of the boundary condition for the tangential flux (Sec. III B). Section IV focuses on the corresponding motion laws for a linear stability analysis with a nonzero $\boldsymbol{B}$ field (Sec. IV A) and a scaling prediction for the perturbed eigenfrequencies when the $\boldsymbol{B}$ field is weak (Sec. IV B). In Sec. V, we carry out numerical simulations (Secs. V A and V B), and discuss their implications (Sec. V C). Section VI provides an overlook and outline of open problems.

Notation and terminology. Throughout the paper, we write $f = \mathcal{O}(g)$ for scalars f and g to mean that $|f/g|$ is bounded by a strictly positive constant in a prescribed limit. We use the term fluid instability spectrum—and fluid stability spectrum—to mean the discrete set of frequencies coming from the linear stability analysis of the governing equations.

II. REVIEW OF DS MODEL

In this section, we review the main ingredients of the DS model [23]. In particular, we describe the problem geometry, equations of motion, and the associated boundary conditions; see Sec. II A. In addition, we review the main result of the linear stability analysis (Sec. II B); and point out a scaling limit (Sec. II D).

A. Geometry and governing equations

The problem geometry is shown in Fig. 1. The electronic fluid occupies an infinitely long channel. The spatial coor-

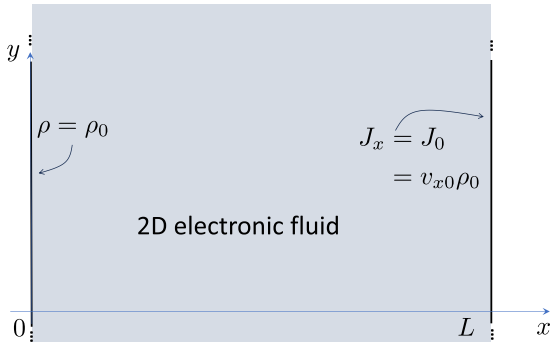

FIG. 1. Geometry of the problem. The electronic fluid lies in an infinite-in-y channel of width L, with edges at $x = 0$ and $x = L$. The electronic density ρ is fixed at the constant value ρ_0 at the left boundary, $x = 0$; and the normal flux J_x has the constant value $J_0 = v_{x0}\rho_0$ at the right boundary, $x = L$.

dinates are (x, y) with $0 < x < L$ and $-\infty < y < +\infty$. The fluid flows in the x direction. The electronic number density per unit area is ρ, and the vector-valued fluid velocity is (v_x, v_y) with $v_y = 0$. The variables ρ and v_x are y independent, and satisfy the system of equations [23]

$$\left(\frac{\partial}{\partial t} + v_x\frac{\partial}{\partial x}\right)v_x = -a\frac{\partial \rho}{\partial x}, \tag{1a}$$

$$\frac{\partial \rho}{\partial t} + \frac{\partial}{\partial x}(\rho\, v_x) = 0, \quad 0 < x < L, \tag{1b}$$

where $a = e^2/(Cm_e)$ is a positive constant ($a > 0$); e is the electron charge ($e > 0$) and C is a quantity expressing the effective capacitance per unit area; $m_e = \bar{m}_e m_{e0}$ is the effective electron mass, and m_{e0} is the free electron mass ($\bar{m}_e = m_e/m_{e0}$). This model comes from the Euler momentum equation and the mass conservation law, where the Lorentz force is $\boldsymbol{F} = (F_x, F_y)$ with $F_y = 0$ and

$$F_x = -e\frac{\partial U}{\partial x}, \quad U \simeq \frac{e\rho}{C}; \tag{1c}$$

and $U(t, x)$ is the electrostatic potential generated by the electronic charge in the channel. The *gradual channel approximation* is applied here, by which the potential $U(t, x)$ is locally proportional to the density $\rho(t, x)$ [33]. We stress that, in this 1D model, $v_y = 0$ everywhere.

In addition, the density ρ and x-directed flux $J_x = \rho v_x$ obey the boundary conditions (see Fig. 1)

$$\left.\begin{aligned} \rho &= \rho_0 = \text{const} \quad \text{at } x = 0, \\ J_x &= v_{x0}\rho_0 = \text{const} \quad \text{at } x = L, \end{aligned}\right\} \tag{2}$$

where ρ_0 and v_{x0} are given positive constants ($\rho_0, v_{x0} > 0$). Thus, the fluid density is kept fixed to a constant at the left boundary ($x = 0$), while the normal flux is fixed to a constant at the right boundary ($x = L$). DS showed that in this setting the sound waves either decay or grow with time as they undergo multiple reflections at the two boundaries [18,23].

B. Linear stability analysis

Let us discuss the particulars of the DS instability. Equations (1) and (2) trivially admit the *uniform* steady-state solution $(v_x, \rho) = (v_{x0}, \rho_0)$. We perturb the fluid system around this solution by setting [23]

$$\rho(t, x) = \rho_0 + \rho_1(x)e^{-\Lambda t}, \quad J_x(t, x) = \rho_0 v_{x0} + \jmath_1(x)e^{-\Lambda t},$$

where the functions ρ_1 and $\jmath_1$ as well as the parameter Λ should be determined consistently with the governing equations. In the notation employed by DS [23], $\Lambda = \mathrm{i}\omega$ where ω is the angular frequency (and $\mathrm{i}^2 = -1$). By linearizing the ensuing equations of motion for $(\jmath_1, \rho_1)$ we find an eigenvalue problem for $-\mathrm{i}\Lambda = \omega$, which is expressed in a matrix form as

$$-\mathrm{i}\mathbb{A}_0\frac{\partial}{\partial x}\begin{pmatrix}\jmath_1\\ \rho_1\end{pmatrix} = \omega\begin{pmatrix}\jmath_1\\ \rho_1\end{pmatrix}, \quad 0 < x < L, \tag{3a}$$

under the homogeneous boundary conditions $\rho_1(0) = 0$ and $\jmath_1(L) = 0$. In the above, $\mathbb{A}_0$ is the 2×2 matrix

$$\mathbb{A}_0 = \begin{pmatrix}2v_{x0} & s_0^2 - v_{x0}^2\\ 1 & 0\end{pmatrix}, \tag{3b}$$

where $s_0 = \sqrt{a\rho_0}$ is the sound speed ($s_0 > 0$). We refer to the ratio $M = v_{x0}/s_0$ as the Mach number (or Mach parameter) of the DS model.

The differential operator for the above eigenvalue problem for the frequency ω is non-Hermitian. Thus, the eigenfrequencies $\omega = -\mathrm{i}\Lambda$ can be complex. Indeed, a direct calculation furnishes [23]

$$\omega = \omega_n = -\mathrm{i}\frac{v_{x0}^2 - s_0^2}{2Ls_0}\left[\ln\left(\frac{v_{x0} + s_0}{v_{x0} - s_0}\right) + \mathrm{i}2n\pi\right]. \tag{4a}$$

Here, n is any integer ($n \in \mathbb{Z}$) and the logarithmic function $\ln(\cdot)$ is allowed to take complex values.

By Eq. (4a) we see that in the supersonic regime, i.e., for $v_{x0} > s_0$, we have $\mathrm{Re}\,\Lambda > 0$, which implies a stable system [23]. In contrast, the fluid is unstable in the subsonic regime ($v_{x0} < s_0$). In particular, by analytic continuation of the $\ln(\cdot)$ function in Eq. (4a) we obtain

$$\omega_n = \mathrm{i}\frac{s_0^2 - v_{x0}^2}{2Ls_0}\left[\ln\left(\frac{s_0 + v_{x0}}{s_0 - v_{x0}}\right) + \mathrm{i}(2n+1)\pi\right]; \tag{4b}$$

thus, $\mathrm{Re}\,\Lambda < 0$ if $v_{x0} < s_0$. In each regime the eigenfrequencies ω_n, viewed as points in the complex ω plane, lie in a straight line parallel to the real axis. In the subsonic case, this line is in the upper half ω plane; whereas in the supersonic case the line is in the lower half ω plane. We refer to the point set $\{\omega_n\}_{n\in\mathbb{Z}}$ as the DS spectrum.

C. Distance between DS spectra

It is worthwhile to define a measure of how far or close the fluid instability and stability spectra are within the DS model. This notion of a "spectral distance" can be used to estimate the effect of kinetics, and can be extended to the case with a nonzero magnetic field.

In the supersonic regime, ω_0 is the eigenfrequency that is closest to the origin of the ω plane. Let us introduce the convenient dimensionless parameter

$$\delta = \frac{1}{2}\left(\frac{v_{x0}^2}{s_0^2} - 1\right) = \frac{1}{2}(M^2 - 1);$$

thus, $\delta > 0$ for stability. Accordingly, we can write the lowest eigenvalue of the stability spectrum, in the supersonic regime, as

$$\omega_0^{\rm DS}(\delta) = -{\rm i}\frac{s_0}{L}\delta \ln\left[\frac{(1+\sqrt{1+2\delta})^2}{2\delta}\right],\ \delta > 0. \tag{5a}$$

In this context, the switch from the supersonic to the subsonic regime can be presented via the replacement of δ by $-|\delta|$. By analytic continuation of the logarithm in the above expression for $\omega_0^{\rm DS}(\delta)$, we obtain the lowest eigenfrequencies of the fluid instability spectrum, viz.,

$$\omega_0^{\rm DS}(-|\delta|) = {\rm i}\frac{s_0}{L}|\delta|\left\{\ln\left[\frac{(1+\sqrt{1-2|\delta|})^2}{2|\delta|}\right] \pm {\rm i}\pi\right\}, \tag{5b}$$

where the double valuedness is because of the unspecified branch for the logarithm. When δ becomes sufficiently small in this expression, the imaginary part dominates and the ambiguity tends to disappear. We can now define the distance $D_\omega^{\rm DS}$ between the fluid stability and instability spectra as a function of the parameter δ by

$$\begin{aligned} D_\omega^{\rm DS}(\delta) &= \left|\omega_0^{\rm DS}(|\delta|) - \omega_0^{\rm DS}(-|\delta|)\right| \\ &\simeq 2\frac{s_0}{L}|\delta|\ \ln\left[\frac{(1+\sqrt{1+2|\delta|})(1+\sqrt{1-2|\delta|})}{2|\delta|}\right]. \end{aligned} \tag{5c}$$

The first line is unambiguous since the result for $D_\omega^{\rm DS}(\delta)$ is the same regardless of the sign choice in Eq. (5b). In the approximation of the second line of Eq. (5c), we neglect the $\pm{\rm i}\pi$ contribution from Eq. (5b). Note that it suffices to consider $\delta > 0$ for the domain of $D_\omega^{\rm DS}(\delta)$.

It is tempting to interpret formula (5c). In particular, we have $D_\omega^{\rm DS}(\delta) \to 0$ as $\delta \to 0$. We conclude that the passage from stability to instability in the DS model is continuous in the Mach number $M = v_{x0}/s_0$, for any system that can exist in both regimes within this hydrodynamic model. In other words, the transition from the lowest eigenvalue of the fluid stability spectrum to its counterpart of the instability spectrum happens continuously with M.

D. Scaling limit

Next, we outline in passing a scaling limit that converts the discrete DS spectrum to a continuous one near the transition point, when $|s_0 - v_{x0}|/s_0$ approaches zero. By inspection of Eq. (4a), we define the wavenumber variable

$$k_n = \frac{({\rm Re}\,\omega_n)}{v_{x0}+s_0} = \frac{v_{x0}-s_0}{s}\frac{n\pi}{L},$$

which has the dimension of inverse length. Note that the plane wave $e^{{\rm i}k_n x}$ describes the spatially slow variation of the fluid density and flux [23]. Evidently, $|k_{n+1} - k_n|L$ is small if $|v_{x0} - s_0|/s_0 \ll 1$. Thus, $k_n = k$ tends to form a continuum of real values in the fluid channel $(0 < x < L)$.

Consider the dimensionless complex frequencies

$$\tilde{\omega}_n = \frac{L\omega_n}{v_{x0}+s_0} = k_n L\left\{1 - \frac{\rm i}{2n\pi}\ln\left(\frac{2n\pi + k_n L}{k_n L}\right)\right\}. \tag{6}$$

In the asymptotic limit with $n \gg 1$ and $k_n L = \mathcal{O}(1)$, we can use the approximation $\tilde{\omega}_n \simeq k_n L$. This limit suggests the continuous real-valued frequency spectrum

$$\omega(k) = (v_{x0}+s_0)k = s_0(M+1)k, \tag{7}$$

which is a linear dispersion relation for the sound waves in this system.

III. FLUID MODEL WITH MAGNETIC FIELD

In this section, we describe the governing hydrodynamic equations with a magnetic field, and determine the corresponding steady state analytically. We investigate two distinct cases of the boundary condition for the tangential flux. We should emphasize that a major difference of this setting with the DS model [23] is that the resulting steady state now becomes spatially dependent.

Consider the geometry of Fig. 1. The electronic fluid is subjected to the out-of-plane, static magnetic field $\boldsymbol{B} = B\boldsymbol{e}_z$ where B is a constant and $\boldsymbol{e}_z$ is the z-directed Cartesian unit vector. The equations of motions form an extension of Eqs. (1a) and (1b) to the setting with the full 2D velocity vector field $\boldsymbol{v} = (v_x, v_y)$ and the Lorentz force $\boldsymbol{F} = e(-\nabla U + \boldsymbol{v}\times\boldsymbol{B})$ under the gradual channel approximation [33]. The shallow-water equations become

$$\left.\begin{aligned} \left(\tfrac{\partial}{\partial t} + v_x\tfrac{\partial}{\partial x} + v_y\tfrac{\partial}{\partial y}\right)v_x &= -a\tfrac{\partial\rho}{\partial x} + \tfrac{e}{m_e}v_y B, \\ \left(\tfrac{\partial}{\partial t} + v_x\tfrac{\partial}{\partial x} + v_y\tfrac{\partial}{\partial y}\right)v_y &= -a\tfrac{\partial\rho}{\partial y} - \tfrac{e}{m_e}v_x B, \\ \tfrac{\partial\rho}{\partial t} + \tfrac{\partial}{\partial x}(\rho\, v_x) + \tfrac{\partial}{\partial y}(\rho\, v_y) &= 0. \end{aligned}\right\} \tag{8}$$

This system of equations must be supplemented with boundary conditions at the channel edges. By generalization of the DS boundary conditions, Eq. (2), we impose

$$\left.\begin{aligned} \rho &= \rho_0 \quad \text{at } x = 0, \\ J_x &= v_x\,\rho = v_{x0}\,\rho_0 \quad \text{at } x = L, \end{aligned}\right\} \tag{9a}$$

where $\boldsymbol{J} = (J_x, J_y)$ is the flux vector. Here, we require that the density ρ and normal flux J_x be held fixed at the left and right boundary, respectively, similarly to the DS setting [23]. Furthermore, we need a boundary condition for the tangential (or, lateral) flux, $J_y = v_y\rho$.

We study the following two scenarios. In *Case I*, J_y takes mutually opposite values at the boundaries, viz.,

$$J_y\big|_{x=0} = -J_y\big|_{x=L}. \tag{9b}$$

Alternatively, in *Case II*, J_y vanishes at the right boundary, viz.,

$$J_y = 0 \quad \text{at } x = L. \tag{9c}$$

The imposition of either Eq. (9b) or (9c) provides a third (scalar) boundary condition in the model.

Condition (9b) is deemed as physically reasonable, since it is consistent with the property that the $\boldsymbol{B}$ field tends to generate a centripetal force on an electron along a circle of diameter L centered at $x = L/2$. Indeed, Case I yields a steady state with $J_y = \pm eBL\rho_0/(2m_e)$ at the two ends of the channel (Sec. III B 1). By our linearized-stability formulation around this steady state, the resulting perturbations of these boundary values come from the related eigenfunctions (eigenmodes) and are not uniquely defined. In an actual physical setting, these values should be determined uniquely at times $t > 0$

via the prescription of suitable initial data (at $t = 0$) for the time-dependent hydrodynamic equations. This task is distinct from our spectral problem. For a discussion, see Sec. V C. On the other hand, condition (9c) of Case II is imposed for comparison purposes. The model of Eqs. (8) and (9a) with Eq. (9b) or (9c) can be complemented with initial conditions for (ρ, J_x, J_y), which we omit here.

A few more remarks are in order. First, the governing differential equations are not invariant under time reversal (by $t \mapsto -t$) if $B \neq 0$. Second, the particular choice of Eq. (9c) yields a system of boundary conditions that closely imitates the DS setting. In this case, the flux vector $\boldsymbol{J}$ near the right boundary tends to locally reduce to the form (const, 0), which resembles the 1D flow of the DS model. This choice is mathematically convenient. For example, with Eq. (9c) the fluid spectrum *smoothly* reduces to that of the DS model in the limit $\boldsymbol{B} \to 0$. In contrast, this limit exhibits an anomaly under condition (9b), as we discuss later on (Sec. V A). Third, for each choice of the boundary condition for J_y, the electronic steady state has a nontrivial dependence on x if $B \neq 0$. This feature contrasts the constant steady state in [23], and dramatically affects the fluid spectrum.

Notice that we have applied the usual convention of particles with a positive charge e (i. e., $e > 0$). The case with a negative charge (if $e \mapsto -e$) leads to dynamics identical to those with fixed positive charge e and flipped sign of B ($B \mapsto -B$). In this latter setting, the mirror symmetry of the governing equations entails that $(\rho, v_x, v_y) \mapsto (\rho, v_x, -v_y)$ with $y \mapsto -y$. In other words, if (ρ, v_x, v_y) is a solution of the model for given B and fixed e then $(\rho, v_x, -v_y)$ must also be a solution if (y, B) is replaced by $-(y, B)$. Thus, it suffices to assume that $B > 0$ throughout. To simplify the analysis, we additionally enforce *translation invariance* and restrict our attention to y-independent solutions, setting

$$\frac{\partial}{\partial y}(\rho, J_x, J_y) = 0 \quad \text{everywhere.} \tag{10}$$

Despite this restriction, the tangential velocity v_y is nonzero in the channel $(0 < x < L)$ if $B \neq 0$.

A. Rescaled variables

Next, we introduce rescaled variables and nondimensionalize the governing equations, for later numerical and algebraic convenience. Recall the quantities ρ_0 and v_{x0}, which are the reference values for the electronic number density and normal velocity from the boundary conditions in Eq. (9a) [23].

First, we introduce a reference magnetic field, $B_0 > 0$. The respective dimensionless parameter β is defined by

$$\beta = B/B_0 > 0.$$

Recall the sound speed $s_0 = \sqrt{a\rho_0}$ (Sec. II B).

We rescale the dependent variables by setting

$$\check{v}_x = \frac{v_x}{v_{x0}}, \quad \check{v}_y = \frac{v_y}{s_0}, \quad \check{\rho} = \frac{\rho}{\rho_0}.$$

The rescaled x coordinate and channel width are

$$\check{x} = \frac{x}{\ell}, \quad \check{l} = \frac{L}{\ell} \quad \text{where } \ell = \frac{s_0 m_e}{eB_0};$$

thus, $0 \leqslant \check{x} \leqslant \check{l}$. Notably, the hydrodynamic quantities $(\check{v}_x, \check{v}_y, \check{\rho})$ are scaled by v_{x0}, s_0, and ρ_0, which are independent of the parameter β and thus of the magnetic field B. This ensures that the rescaling remains well defined in the limit $\beta \to 0$. We will fix the reference field B_0 by setting $\check{l} = 1$ for our numerics (Sec. V). This value entails $B_0 = \frac{s_0 m_e}{eL}$, which yields a conversion formula for the frequencies of the fluid spectrum, as discussed in Sec. V C. For the sake of generality, we use an arbitrary yet β-independent $\check{l}$ ($\check{l} > 0$) in the present section and in Sec. IV.

The equations of motion in the scaled variables read

$$\left.\begin{aligned} \left(\tfrac{\partial}{\partial \check{t}} + \check{v}_x \tfrac{\partial}{\partial \check{x}}\right)\check{v}_x &= M^{-2}\left(-\tfrac{\partial \check{\rho}}{\partial \check{x}} + \beta\, \check{v}_y\right), \\ \left(\tfrac{\partial}{\partial \check{t}} + \check{v}_x \tfrac{\partial}{\partial \check{x}}\right)\check{v}_y &= -\beta\, \check{v}_x, \\ \tfrac{\partial \check{\rho}}{\partial \check{t}} + \tfrac{\partial}{\partial \check{x}}(\check{\rho}\, \check{v}_x) &= 0, \end{aligned}\right\} \tag{11}$$

where (for $M = v_{x0}/s_0$)

$$\check{t} = \frac{v_{x0}}{\ell} t = M \frac{eB_0}{m_e} t.$$

In view of conditions (9b) and (9c), Eq. (11) is subject to one of the following two sets of boundary conditions. Case I corresponds to

$$\left.\begin{aligned} &\check{\rho} = 1 \quad \text{at } \check{x} = 0, \\ &\check{J}_x = \check{v}_x\, \check{\rho} = 1 \quad \text{at } \check{x} = \check{l}, \\ &\check{J}_y\big|_{x=0} + \check{J}_y\big|_{x=\check{l}} = 0. \end{aligned}\right\} \tag{12}$$

Case II amounts to

$$\left.\begin{aligned} &\check{\rho} = 1 \quad \text{at } \check{x} = 0, \\ &\check{J}_x = \check{v}_x\, \check{\rho} = 1, \quad \check{J}_y = \check{v}_y \check{\rho} = 0 \quad \text{at } \check{x} = \check{l}. \end{aligned}\right\} \tag{13}$$

B. Steady-state solution for $B \neq 0$

The magnetically driven system of Eq. (11) together with Eq. (12) or (13) admits a time-independent solution, which we will describe in the rescaled variables $(\check{\rho}, \check{v}_x, \check{v}_y)$ for each choice of the boundary condition for $\check{J}_y$. For details on the analytical derivation, see Appendix A.

1. Exact steady state

Let $(\check{\rho}^s, \check{v}_x^s, \check{v}_y^s)$ denote the steady-state solution. We distinguish two cases.

Case I: Mutually opposite boundary values of lateral flux. Let us consider a time-independent solution to Eqs. (11) and (12). After some algebra, this solution is cast into the following algebraic form (for $0 \leqslant \check{x} \leqslant \check{l}$),

$$\begin{aligned} &\check{v}_x^s(\check{x}) = (\check{\rho}^s(\check{x}))^{-1}, \quad \check{v}_y^s(\check{x}) = \beta\left(\frac{\check{l}}{2} - \check{x}\right), \\ &\check{\rho}^s(\check{x}) = b^{1/3}\, \epsilon(\check{x})^{-2/3} \left\{\frac{2}{3}\cos\left(\frac{\theta(\check{x})}{3}\right) + \frac{1}{3}\right\}. \end{aligned} \tag{14}$$

Here, we set $b = \frac{1}{2}M^2 = \frac{1}{2}\frac{v_{x0}^2}{s_0^2} > 0$,

$$\epsilon(\check{x}) = \frac{\sqrt{b}}{\left[1 + b + \frac{\beta^2}{2}\check{x}(\check{l} - \check{x})\right]^{3/2}}, \tag{15}$$

and by using a suitable analytic continuation of the inverse cosine (Appendix A), we introduce the functions

$$\theta(\check{x}) = \begin{cases} \cos^{-1}\left(1 - \frac{27}{2}\epsilon(\check{x})^2\right), & \text{for } b < \frac{1}{2}, \\ 2\pi - \cos^{-1}\left(1 - \frac{27}{2}\epsilon(\check{x})^2\right), & \text{for } b > \frac{1}{2}. \end{cases} \tag{16}$$

In the above, the function $\cos^{-1}(\cdot)$ takes (real) values only in its principal branch $[0 \leqslant \cos^{-1}(\cdot) < \pi]$. The cases with $b < 1/2$ and $b > 1/2$ amount to $v_{x0} < s_0$ and $v_{x0} > s_0$, respectively. We still refer to these cases as the subsonic and supersonic regime, respectively. Evidently, by Eqs. (14)–(16), the variables $\check{\rho}^s$ and $\check{v}_x^s$ are symmetric (i.e., even) with respect to the channel center, $\check{x} = \check{l}/2$; whereas $\check{v}_y^s$ is antisymmetric (odd). Notice that the sign of $\check{v}_y^s$ is reversed but $\check{v}_x^s$ and $\check{\rho}^s$ remain invariant if the sign of either B or e is switched, as expected by the mirror symmetry of the governing equations. If $B \to 0$, this solution continuously reduces to that of the DS model [23]; for example, notice that $\check{v}_y \to 0$ as $B \to 0$.

Case II: Zero lateral flux at the right boundary. We seek a time-independent solution to Eqs. (11) and (13). By analogy with Eqs. (14) and (15), we obtain

$$\begin{aligned} &\check{v}_x^s(\check{x}) = (\check{\rho}^s(\check{x}))^{-1}, \quad \check{v}_y^s(\check{x}) = \beta\,(\check{l} - \check{x}), \\ &\check{\rho}^s(\check{x}) = b^{1/3}\,\epsilon(\check{x})^{-2/3}\left\{\frac{2}{3}\cos\left(\frac{\theta(\check{x})}{3}\right) + \frac{1}{3}\right\}, \end{aligned} \tag{17}$$

and

$$\epsilon(\check{x}) = \frac{\sqrt{b}}{\left[1 + b + \frac{\beta^2}{2}\check{x}(2\,\check{l} - \check{x})\right]^{3/2}}, \tag{18}$$

where $\theta(\check{x})$ is defined by Eq. (16). Note that in this case the tangential velocity $\check{v}_y^s$ results from its counterpart in Eq. (14) by a mere shift of $\check{x}$ by $\check{l}/2$, i.e., $\check{x} \mapsto \check{x} - \check{l}/2$. On the other hand, the $\check{x}$ dependence of $\epsilon(\check{x})$ comes from the appropriate integration of $\check{v}_y^s(\check{x})$ (see Appendix A). Again, as $B \to 0$, this solution continuously reduces to that of the DS model [23].

An interesting, yet not surprising, mathematical feature of the above steady states should be pointed out. The distinct effect of each kinetic (subsonic or supersonic) regime can be connected to a particular branch of an intrinsically multivalued function, namely, the generalized inverse cosine $\cos^{-1} z$, as is indicated by the definition of $\theta(\check{x})$; see Appendix A. This *branching* is manifested in the steady-state normal velocity and density; in contrast, the lateral velocity does not distinguish between the two regimes. For fixed β and $\check{x}$ ($\check{x} \neq 0,\ \check{l}$), we see that the steady-state density and normal flux as a function of b exhibit a jump at the transition point, $b = 1/2$. This structure of the steady state endows the magnetic fluid system with linear stability and instability spectra qualitatively different from those of the DS case ($B = 0$), as discussed in Sec. V. We should mention that, for Case I, in the limit $\beta \to 0$ ($B \to 0$) the fluid spectrum exactly reduces to the union of the spectrum of the DS model and a spectrum of geometric character with a nonzero lateral flux in the channel. This limit is discussed in Secs. V C and VI.

2. *Asymptotics for weak magnetic field, $|\beta|\check{l} \ll 1$*

Formulas (14) and (17) are simplified for a weak magnetic field (see Appendix A). By inspection of Eqs. (15) and (18), we realize that the relevant parameter is

$$\beta\check{l} = \frac{eBL}{s_0 m_e},$$

which expresses the strength of the magnetic Lorentz force with magnitude $es_0|B|$ relative to the mechanical (centripetal-like) intrinsic force of magnitude $m_e s_0^2/L$ on an electron. The assumption for a weak magnetic field means that the latter force dominates, i.e., $|\beta\check{l}| \ll 1$. Consider β as real (positive or negative) in this section.

It turns out that the approximation for $\check{\rho}^s$ also depends on the proximity of the kinetics to the transition point, $b = 1/2$. In fact, for $|\beta|\check{l} \ll 1$ and arbitrary positive b, we distinguish the cases with $|\beta|\check{l} \ll \sqrt{|1 - 2b|}$ and $\beta\check{l} = \mathcal{O}(\sqrt{|1 - 2b|})$. In the former case, we can simplify $\check{\rho}^s$ by regular perturbations, ignoring the transition point. In the latter case, $\check{\rho}^s$ is amenable to singular perturbations since the kinetics of the transition point, if b is near $1/2$, significantly interfere with perturbations in β.

Consider $\beta\check{l} \ll \sqrt{|1 - 2b|}$, which signifies an *extremely weak* magnetic field. Let us discuss the scenario of Case I. By Eq. (14), we calculate (see Appendix A)

$$\check{\rho}^s(\check{x}) \simeq 1 + \frac{\beta^2}{2(1 - 2b)}\check{x}(\check{l} - \check{x}), \quad 0 \leqslant \check{x} \leqslant \check{l}, \tag{19a}$$

which is recognized as a regular perturbation of the DS steady state. Notice the absence of a linear-in-β term in the above expansion, as expected because the sign reversal of B leaves $\check{\rho}^s$ invariant. Similarly, the rescaled normal velocity, $\check{v}_x^s = (\check{\rho}^s)^{-1}$, exhibits an $\mathcal{O}(\beta^2\check{l}^2)$ correction to its DS steady-state value, for $\beta = 0$. On the other hand, we have $\check{v}_y^s = \beta(\check{l}/2 - \check{x})$.

Next, consider $\beta\check{l} = \mathcal{O}(\sqrt{|1 - 2b|})$, which provides a critical scaling for β near the transition point. By Eq. (14), we obtain (see Appendix A)

$$\check{\rho}^s(\check{x}) \simeq 1 + \frac{|\beta|}{\sqrt{3}}\,\mathrm{sgn}(1 - 2b)\sqrt{\check{x}(\check{l} - \check{x})}, \tag{19b}$$

for $0 \leqslant \check{x} \leqslant \check{l}$. In the above, sgn denotes the signum function; $\mathrm{sgn}(x) = 1$ if $x > 0$ and $\mathrm{sgn}(x) = -1$ if $x < 0$. Asymptotic formulas (19a) and (19b) are distinct and nonoverlapping. These expressions are connected only through the more complicated Eqs. (14) and (16).

The scenario of Case II, which leads to Eq. (17), can be studied similarly. Formulas (19a) and (19b) are applicable with the factor $\check{x}(\check{l} - \check{x})$ replaced by $\check{x}(2\check{l} - \check{x})$.

IV. LINEAR STABILITY FORMULATION

In this section, by linear stability theory we formulate an eigenvalue problem for the model based on Eqs. (11) and (12), or Eqs. (11) and (13), with $\beta \neq 0$. We derive a system of

linear equations for the hydrodynamic variables, and discuss its properties for a sufficiently weak magnetic field. For more details, see Appendix B.

In the spirit of Sec. II B for the DS model, let us consider the scaled (dimensionless) flux vector $(\check{J}_x, \check{J}_y) = (\check{\rho}\check{v}_x, \check{\rho}\check{v}_y)$ and density $\check{\rho}$, and perturb them around a steady-state solution of Sec. III B. Hence, we write

$$(\check{J}_x, \check{J}_y) = (\check{J}^s_x(\check{x}), \check{J}^s_y(\check{x})) + (\check{\jmath}_1(\check{x}), \check{\jmath}_2(\check{x}))e^{-\check{\Lambda}\check{t}},$$

where $(\check{J}^s_x, \check{J}^s_y) = (\check{\rho}^s\check{v}^s_x, \check{\rho}^s\check{v}^s_y)$, while

$$\check{\rho} = \check{\rho}^s(\check{x}) + \check{\rho}_1(\check{x})e^{-\check{\Lambda}\check{t}}, \quad 0 < \check{x} < \check{l}.$$

In the above, the physically admissible values of the parameter $\check{\Lambda}$ must be determined consistently with the governing equations of motion and boundary conditions for the perturbation variables $\check{\rho}_1$, $\check{\jmath}_1$, $\check{\jmath}_2$. Note that $\check{\Lambda}$ is dimensionless; its dimensional counterpart Λ has units of inverse time (or, frequency) and is related to $\check{\Lambda}$ by

$$\Lambda = \frac{eB_0 v_{x0}}{m_e s_0}\check{\Lambda} = \frac{eB_0\sqrt{2b}}{m_e}\check{\Lambda}.$$

Recall that in the rescaled variables the time is expressed via $\check{t}$ in units of $\frac{m_e}{eB_0}\frac{s_0}{v_{x0}}$, which equals $\frac{L}{v_{x0}}$ if $\check{l} = 1$. Since $\Lambda = \mathrm{i}\omega$, we write $\check{\Lambda} = \mathrm{i}\check{\omega}$ with the rescaled frequency $\check{\omega} = \frac{m_e s_0}{eB_0 v_{x0}}\omega$, which becomes $\check{\omega} = \frac{L}{v_{x0}}\omega$ for $\check{l} = 1$.

A. Governing motion laws

The formulation with rescaled variables is summarized as follows. First, the systems of Eqs. (11) and (12), and Eqs. (11) and (13) are converted to systems of nonlinear equations for the vector-valued function $(\check{J}_x, \check{J}_y, \check{\rho})$, as shown in Appendix B. By linearizing each system of governing equations around the corresponding steady state, we obtain in matrix form the related eigenvalue problem for $\check{\Lambda}$ and the vector-valued function $\overline{U}(\check{x}) = (\check{\jmath}_1(\check{x}), \check{\jmath}_2(\check{x}), \check{\rho}_1(\check{x}))^T$ where the subscript T denotes the transpose of a vector, viz.,

$$\frac{\partial}{\partial\check{x}}\{\mathbb{A}(\check{x})\overline{U}(\check{x})\} + \beta\mathbb{B}\,\overline{U}(\check{x}) = \mathrm{i}\,\check{\omega}\,\overline{U}(\check{x}), \tag{20}$$

where

$$\mathbb{A}(\check{x}) = \begin{pmatrix} 2\check{v}^s_x & 0 & \frac{\check{\rho}^s}{2b} - (\check{v}^s_x)^2 \\ \check{v}^s_y & \check{v}^s_x & -\check{v}^s_x\check{v}^s_y \\ 1 & 0 & 0 \end{pmatrix}, \quad \mathbb{B} = \begin{pmatrix} 0 & -\frac{1}{2b} & 0 \\ 1 & 0 & 0 \\ 0 & 0 & 0 \end{pmatrix},$$

for $0 < \check{x} < \check{l}$. Recall that the functions $\check{\rho}^s$, $\check{v}^s_x$, and $\check{v}^s_y$ depend on β. We also apply the following boundary conditions:

$$\text{Case I}: \ \check{\rho}_1(0) = 0, \ \check{\jmath}_1(\check{l}) = 0, \ \check{\jmath}_2(0) = -\check{\jmath}_2(\check{l}); \tag{21}$$

or, alternatively,

$$\text{Case II}: \ \check{\rho}_1(0) = 0, \ \check{\jmath}_1(\check{l}) = 0, \ \check{\jmath}_2(\check{l}) = 0. \tag{22}$$

Equation (20) together with Eq. (21) or (22) should yield the desired sets of eigenfrequencies $\check{\omega}$. We have been unable to solve these eigenvalue problems analytically, because of the complicated dependence of $\mathbb{A}(\check{x})$ on $\check{x}$ via the steady-state solution. In Sec. V, we present numerical computations for the stability and instability spectra, and compare related features of Cases I and II.

B. Scaling law for extremely weak magnetic field

Next, we outline how the deviation of the rescaled eigenfrequency $\check{\omega}$ for $\beta \neq 0$ from its corresponding unperturbed value $\check{\omega}^0$ of the DS model scales with β if $(\beta\check{l})^2 \ll |1 - 2b|$. We invoke results of Sec. III B 2 for the expansion of the steady state. Our discussion here concerns both eigenvalue problems of Sec. IV A. For small $|\beta|$, we expand the solution of the linearized model around the DS solution for the fields and spectrum.

We use the fact that the steady-state solution has an expansion in integer powers of β in this asymptotic regime. Consequently, the matrix $\mathbb{A}(\check{x})$ of Eq. (20) admits a similar expansion in powers of β. We apply regular perturbation theory to the ensuing system of equations. Hence, in Eq. (20) we try the formal expansions

$$\overline{U} \simeq \overline{U}_0 + \beta^c\,\overline{\mathfrak{U}}, \quad \check{\omega} \simeq \check{\omega}^0 + \beta^\nu\,\check{\omega}^{dev}.$$

Here, $(\overline{U}_0, \check{\omega}^0)$ represents the rescaled solution of the DS model, the unknown coefficients $\overline{\mathfrak{U}}$ and $\check{\omega}^{dev}$ are assumed independent of β, and the exponents c and ν must be determined consistently with the governing equations. In this procedure, we take into account that $\overline{U}_0$ has zero lateral flux ($\check{\jmath}_{2,0} = 0$ everywhere), and the matrix $\mathbb{B}$ is independent of β while $\mathbb{A} = \mathbb{A}_0 + \beta\mathbb{A}_1 + \ldots$ where $\mathbb{A}_1$ is sparse with zero first and third rows. After some algebra, dominant-balance arguments yield $c = 1$ and $\nu = 2$, with $\overline{\mathfrak{U}}$ containing only one nonzero component in the interior of the channel, namely, the lateral flux. These findings are compatible with the mirror symmetry of the governing motion laws (when $\beta \mapsto -\beta$).

Hence, we reach the conclusion that

$$\check{\omega} - \check{\omega}^0 = \mathcal{O}(\beta^2\check{l}^2) \quad \text{if } (\beta\check{l})^2 \ll |1 - 2b|, \tag{23}$$

for each case of the boundary condition for the tangential flux, where $\check{\omega}^0$ corresponds to the DS spectrum. This scaling prediction is corroborated by numerical simulations (Sec. V). We expect that this prediction is modified in the regime where $(\beta\check{l})^2 = \mathcal{O}(|1 - 2b|)$. This case requires the application of singular perturbations to the governing equations, and is not treated here.

V. COMPUTED SPECTRA AND GAP

In this section, we numerically solve the eigenvalue problem described by Eq. (20) with the boundary conditions of Eq. (21) or (22), for Case I or II, respectively. For this purpose, we discretize the related differential operator with a stabilized finite difference scheme. Our numerical method achieves a well-controlled discretization error. For details on the procedure, see Appendix C.

First, we provide numerical results for the instability and stability spectra, i.e., the complex eigenfrequencies $\check{\omega}$, for different values of the parameters β and $\delta = b - 1/2$. The former parameter expresses the strength of the magnetic field and the latter measures the deviation from the transition point. For our numerical computations, we have set $\check{l} = 1$ throughout. Second, we compute the magnetically controlled spectral gap,

showing numerically how this varies with β and δ. Thirdly, we discuss implications of our results.

A. Discrete frequency spectrum

Figure 2 shows sequences of numerically computed, discrete eigenfrequencies for the eigenvalue problem of Case I. This problem is expressed by Eq. (20) and the boundary conditions of Eq. (21). Correspondingly, Fig. 3 shows results of our computation for Case II. The underlying problem is described by Eq. (20) and the boundary conditions of Eq. (22). For both cases, the eigenfrequencies are computed for varying parameters β and δ. In Figs. 2 and 3, each plot [(a)–(e)] contains eigenfrequencies for a fixed magnetic field with the following values: (a) $\beta = 0$, (b) $\beta = 1/64$, (c) $\beta = 1/32$, (d) $\beta = 1/16$, and (e) $\beta = 1/8$. We relate this choice of parameter values to dimensional quantities in Sec. V C.

We compute same-$|\delta|$ pairs of eigenfrequencies of the stability spectrum (for $\delta > 0$) and the instability spectrum ($\delta < 0$) with decreasing values $|\delta| = 1/8, 1/16, 1/32, 1/64, 1/128, 1/256, 1/512$ for the deviation from the transition point. The eigenfrequencies of the stability spectrum (for $\delta > 0$) are located in the lower half-plane since they have negative imaginary part (shaded green regions in Figs. 2 and 3); whereas the eigenfrequencies of the instability spectrum ($\delta < 0$) lie in the upper half-plane (shaded red regions in Figs. 2 and 3).

For $\beta > 0$, Cases I and II of the lateral-flux boundary conditions yield distinct spectra. In both cases, we observe the emergence of a *gap*, defined in Sec. V B, across the transition point in the imaginary parts of the eigenfrequencies of the stability and instability spectra. This gap expresses an *exclusion zone* (strip) that is parallel to the real axis and separates the stability spectrum of eigenfrequencies ($\delta > 0$) from the instability spectrum ($\delta < 0$). We discuss aspects of this gap in Sec. V B.

For Case I, we notice that a part of the numerically computed spectrum is real valued and distinct from the DS prediction if $\beta = 0$. This part, which remains real valued even when β is nonzero, is referred to as the *extraneous spectrum*. We provide a justification for this characterization in Sec. V C. These real eigenfrequencies are denoted by $\breve{\omega}_n^e(\beta, \delta)$, and are continuous with β; thus, there is no growth or decay associated with these frequencies. In Appendix D, we derive this extraneous spectrum in the limit $\beta \to 0$ of our magnetically driven model. For $\beta = 0$, the extraneous eigenfrequencies turn out to be δ-independent, $\breve{\omega}_n^e(0, \delta) = \breve{\omega}_n^{e,0} = (2n+1)\pi$ with $n \in \mathbb{Z}$ (see Appendix D). In Fig. 4, we plot the deviation of the lowest positive eigenvalue, $\breve{\omega}_0^e(\beta, \delta)$, of the extraneous spectrum from its nonmagnetic counterpart, $\breve{\omega}_0^{e,0} = \pi$, as a function of $\mathrm{sgn}(\delta)\beta$ for different values of δ ($\beta > 0$). Note that there is no eigenfrequency of the extraneous spectrum shown in Fig. 2, as all these frequencies lie outside of our plotting domain. In Case II, the nonmagnetic limit of the spectrum is identical to that of the DS model [23]. In contrast, in Case I the resulting (nonmagnetic) spectrum is the union of two sets. One part is the (complex-valued) DS spectrum. The other, real valued, extraneous part is because of a geometric resonance inherent to the lateral-flux boundary condition. This spectrum

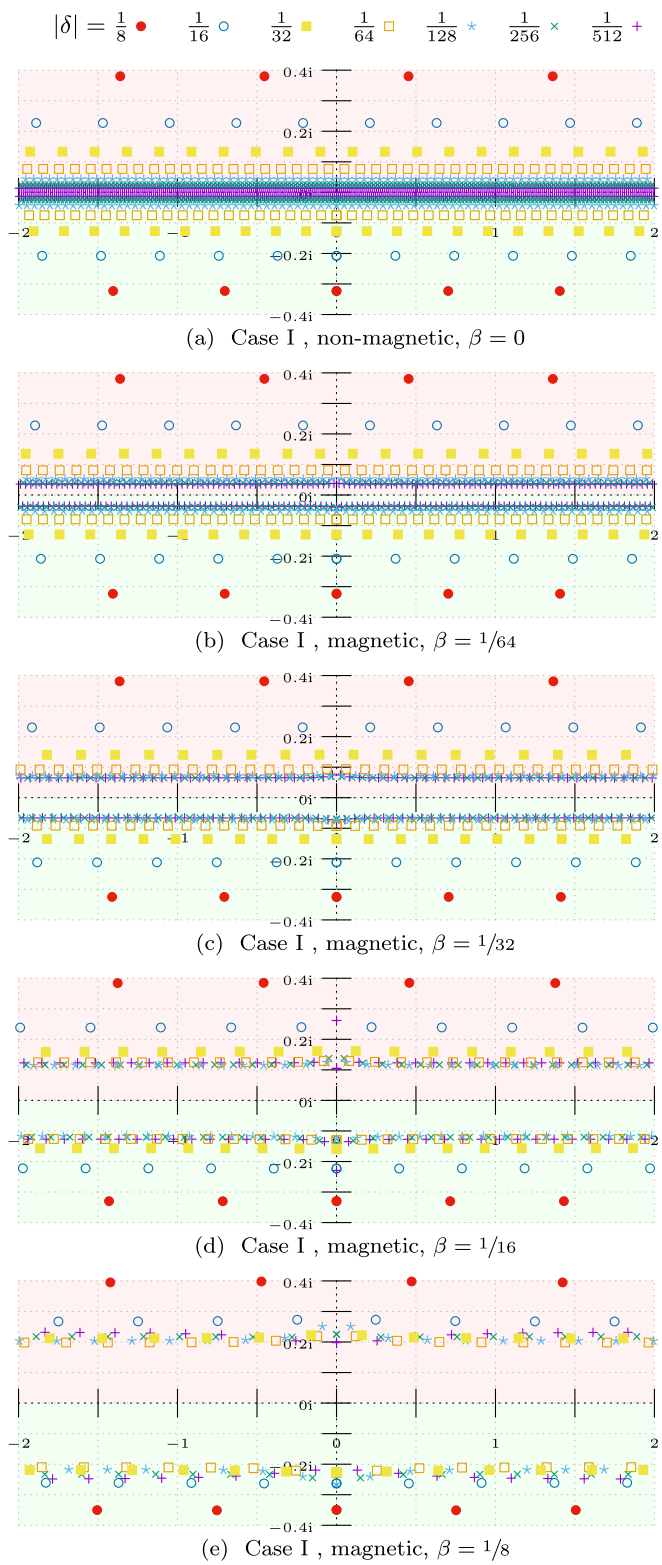

FIG. 2. Case I: Computed eigenfrequencies $\breve{\omega}_n$ from the eigenvalue problem of Eqs. (20) and (21). The magnetic field related values are $\beta = 0, 1/64, 1/32, 1/16, 1/8$; and the kinetic parameter values are $\delta = \pm 1/8, \pm 1/16, \pm 1/32, \pm 1/64, \pm 1/128, \pm 1/256, \pm 1/512$. The green (red) regions contain eigenfrequencies of the stability (instability) spectrum, for $\delta > 0$ ($\delta < 0$).

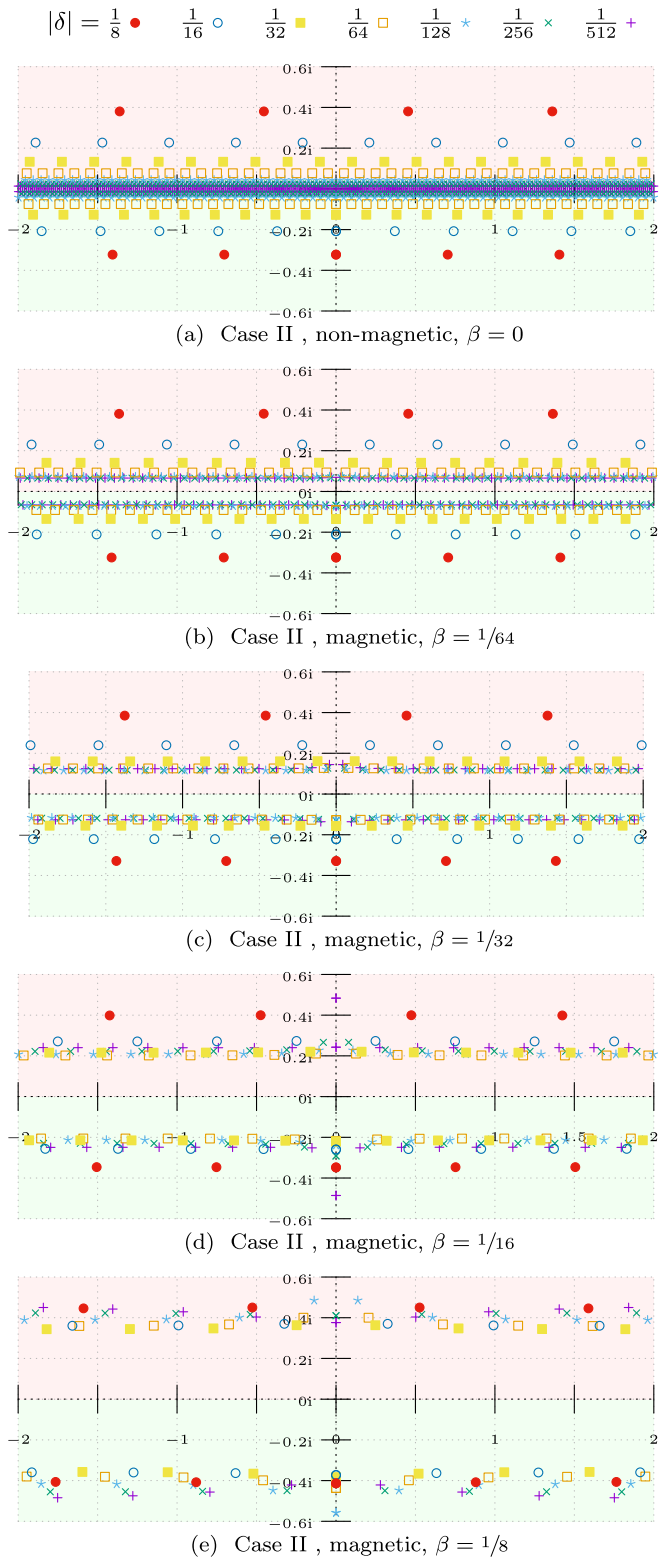

FIG. 3. Case II: Computed eigenfrequencies $\breve{\omega}_n$ from the eigenvalue problem of Eqs. (20) and (22). The magnetic field related values are $\beta = 0$, 1/64, 1/32, 1/16, 1/8; and the kinetic parameter values are $\delta = \pm 1/8$, $\pm 1/16$, $\pm 1/32$, $\pm 1/64$, $\pm 1/128$, $\pm 1/256$, $\pm 1/512$. The green (red) regions contain eigenfrequencies of the stability (instability) spectrum, for $\delta > 0$ ($\delta < 0$).

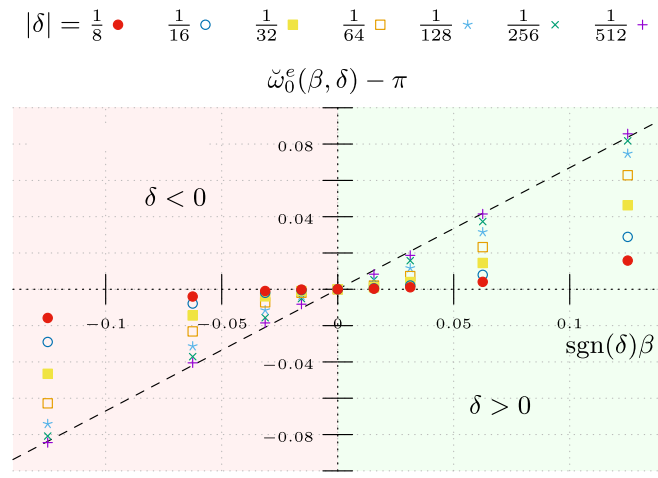

FIG. 4. Case I: Deviation of the lowest positive eigenfrequency $\breve{\omega}_0^e(\beta, \delta)$ of the extraneous spectrum from its nonmagnetic value $\breve{\omega}_0^{e,0} = \breve{\omega}_0^e(0, \delta) = \pi$ as a function of $\mathrm{sgn}(\delta)\beta$ ($\beta > 0$). The numerical values of the kinetic parameter are $\delta = \pm 1/8$, $\pm 1/16$, $\pm 1/32$, $\pm 1/64$, $\pm 1/128$, $\pm 1/256$, $\pm 1/512$. As $|\delta|$ decreases, $\breve{\omega}_0^e(\beta, \delta) - \pi$ asymptotically approaches a straight line (dashed line).

is accompanied by sinusoidal lateral fluxes of wavelengths $L/|n + \frac{1}{2}|$ (Appendix D).

B. Anatomy of spectral gap

Next, we quantitatively define the notion of the spectral gap mentioned above. Consider a given, fixed kinetic parameter $|\delta|$ and magnetic field $\beta > 0$. We define the *spectral distance*, $D_{\breve{\omega}}(\beta, \delta)$, as follows: Subtract the (strictly negative) maximum of the imaginary parts of all computed eigenfrequencies of the stability spectrum from the (strictly positive) minimum of the imaginary parts of all eigenfrequencies of the instability spectrum. This operation implies the following formula:

$$D_{\breve{\omega}}(\beta, \delta) = \min_n \{\mathrm{Im}\, \breve{\omega}_n(-|\delta|) > 0\} - \max_n \{\mathrm{Im}\, \breve{\omega}_n(|\delta|) < 0\}. \tag{24}$$

This definition of the spectral distance is an extension of the spectral distance $D_{\tilde{\omega}}^{\mathrm{DS}}(\delta)$ introduced in Eq. (5c), for the DS model. Recall the related scaled eigenfrequencies $\tilde{\omega}_n$ of Eq. (6). The definition of Eq. (24) excludes the extraneous spectrum, which is present in Case I.

In Fig. 5, we show the effects of the kinetic deviation parameter δ and magnetic field β on the computed spectral distance, $D_{\breve{\omega}}(\beta, \delta)$, for the values $\beta =$ 0, 1/64, 1/32, 1/16, 1/8. For the sake of comparisons, in Fig. 5 we also plot the function $D_{\tilde{\omega}}^{\mathrm{DS}}(\delta)$, which signifies the nonmagnetic limit, when $\beta = 0$, corresponding to the DS model (dashed-red curve). We verify that the numerically computed spectral distance with $\beta = 0$ agrees with formula (5c) for $D_{\tilde{\omega}}^{\mathrm{DS}}(\delta)$; this function is monotone in δ with $D_{\tilde{\omega}}^{\mathrm{DS}}(\delta) \to 0$ as $\delta \to 0$.

For $\beta > 0$, we define the *spectral gap* $G_{\breve{\omega}}(\beta)$ as follows:

$$G_{\breve{\omega}}(\beta) = \min_{\delta > 0} D_{\breve{\omega}}(\beta, \delta) > 0, \tag{25}$$

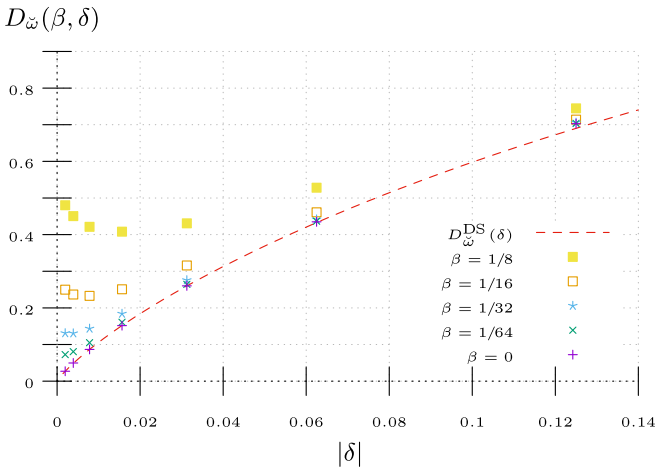

(a) Case I

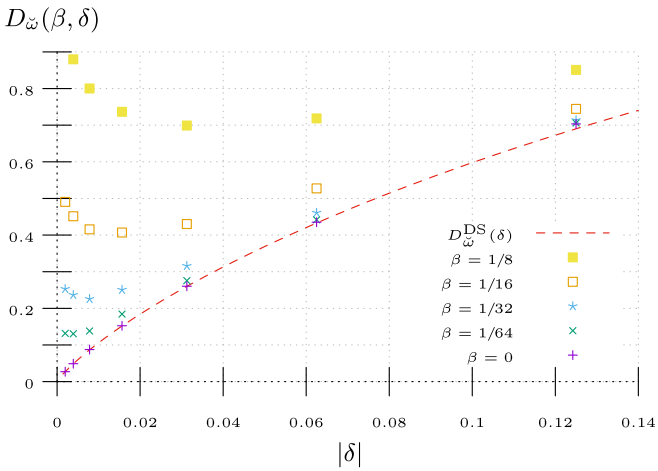

(b) Case II

FIG. 5. Spectral distance $D_{\breve{\omega}}(\beta, \delta)$, given by Eq. (24), as a function of kinetic parameter $|\delta|$, for several values of β ($0 \leqslant \beta \ll 1$), for Case I [(a)] and Case II [(b)]. Dashed red curve: The respective plot of $D_{\breve{\omega}}^{\mathrm{DS}}(\delta)$, for the reference case of the DS model, by use of Eq. (5c).

which is strictly positive in the presence of a (nonzero) magnetic field. An inspection of Fig. 5 suggests that for Case I we have

$$G_{\breve{\omega}}(1/8) \approx 0.41, \quad G_{\breve{\omega}}(1/16) \approx 0.23,$$
$$G_{\breve{\omega}}(1/32) \approx 0.13, \quad G_{\breve{\omega}}(1/64) \approx 0.07.$$

For Case II, the corresponding values are

$$G_{\breve{\omega}}(1/8) \approx 0.70, \quad G_{\breve{\omega}}(1/16) \approx 0.41,$$
$$G_{\breve{\omega}}(1/32) \approx 0.24, \quad G_{\breve{\omega}}(1/64) \approx 0.13.$$

Lastly, we provide numerical evidence for the heuristically derived β^2-scaling law regarding the deviation of the eigenfrequencies from their nonmagnetic limit of the DS model under an extremely weak magnetic field (Sec. III B 2). To this end, we compute the difference $D_{\breve{\omega}}(\beta, \delta) - D_{\breve{\omega}}^{\mathrm{DS}}(\delta)$ for fixed $\delta = \delta_*$ and as a function of the extremely weak magnetic field, when $\beta\breve{l} \ll \sqrt{2|\delta|}$. The numerical results are displayed in Fig. 6. Evidently, the scaling prediction of Eq. (23) ceases

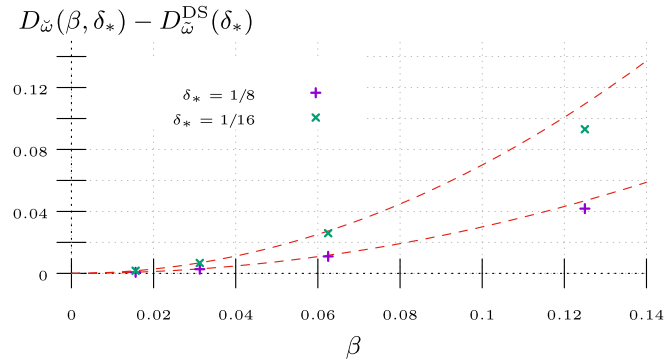

(a) Case I

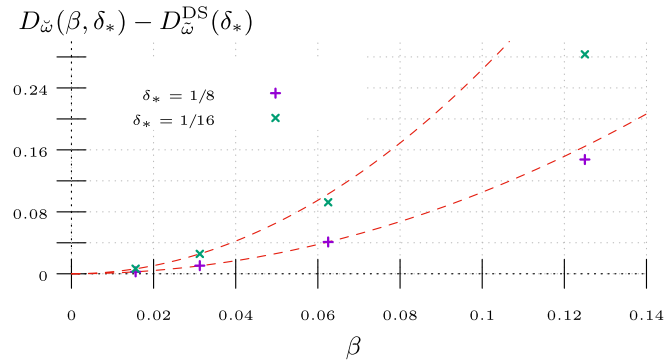

(b) Case II

FIG. 6. Numerical evidence for scaling law (23). Computed $D_{\breve{\omega}}(\beta, \delta_*) - D_{\breve{\omega}}^{\mathrm{DS}}(\delta_*)$ vs β with $\beta\breve{l} \ll \sqrt{2|\delta|}$, for fixed values $\delta_* = 1/8$ and $\delta_* = 1/16$, for Case I [(a)] and Case II [(b)]. Dashed red curve: Best fit to a parabola of form $C\beta^2$, in view of Eq. (23).

to follow the numerically computed values if β^2 becomes sufficiently large.

C. Discussion of results

Although our computations are restricted to relatively weak magnetic fields in the linear regime of the shallow-water equation model, the results may have more general implications. We believe that we predict trends that persist even in cases with large magnetic perturbations, away from the critical transition point, $b = 1/2$ (or, $\delta = 0$).

There are two main predictions indicated by our numerics. Notably, in the instability regime the growth exponents increase with β; and a spectral gap is present near the transition point. We discuss these observations below (Sec. V C 1). In addition, we discuss the meaning of the extraneous spectrum for Case I (Sec. V C 2).

1. Growth exponents and spectral gap

It is of interest to relate the values of the dimensionless parameters used in our numerical computations to dimensional physical quantities, in the context of the shallow-water equations. Let s_0/L and $\bar{m}_e$ (ratio of effective mass m_e to free electron mass m_{e0}) be free parameters, without specifying the 2D material. For $\breve{l} = 1$, by the definitions of B_0 and rescaled

frequency $\breve{\omega}$ we find

$$\omega_n = \breve{\omega}_n \sqrt{1+2\delta}\,\frac{s_0}{L}, \quad B_0 = \frac{m_{e0}}{e}\bar{m}_e\,\frac{s_0}{L},$$

with $B = \beta B_0$. Note that B_0, and thus B for given β, is proportional to $\bar{m}_e$. For the values of β and δ in our numerics, the real parts of the computed frequencies $\breve{\omega}_n$ may lie in the appealing range of THz if s_0/L takes suitable values. For example, consider s_0/L between 0.5 THz and 10 THz. Consequently, we would have $2.8\bar{m}_e\,\mathrm{T} \lesssim B_0 \lesssim 57\bar{m}_e\,\mathrm{T}$, which amounts to

$$0.5\breve{\omega}_n\,\mathrm{THz} \lesssim \frac{\omega_n}{\sqrt{1+2\delta}} \lesssim 10\breve{\omega}_n\,\mathrm{THz} \tag{26}$$

where $-1/2 < \delta < 0$ in the subsonic regime. Relation (26) does not involve $\bar{m}_e$; and may be used near the transition point, for small $|\delta|$, if this kinetic regime is accessible. For $\beta = 1/8$, the largest value of β in our numerics, we obtain $0.35\bar{m}_e\,\mathrm{T} \lesssim B \lesssim 7\bar{m}_e\,\mathrm{T}$. For fixed channel width, e.g., $L = 1\,\mu\mathrm{m}$, a range for s_0 ensues, e.g., $0.5 \times 10^6\,\mathrm{m/s} \lesssim s_0 \lesssim 10^7\,\mathrm{m/s}$.

Our discussion here relies on the assumption that the indicated values of δ are physically accessible within the model of the Euler equations. We have been unable to propose with certainty a specific 2D material that can serve this purpose when $|\delta|$ is small. Hence, the feasibility of observing the predicted spectral gap is left open.

On the other hand, an inspection of Figs. 2, 3, and 6 suggests that the growth exponents, i.e., the imaginary parts of the eigenfrequencies in the instability spectrum, increase with β away from the critical point. This prediction, if extended deeply into the subsonic regime (for δ close to $-1/2$), may plausibly be testable in 2D materials already proposed for the DS instability; see, e.g., [31].

Therefore, for fixed channel width and Mach number of the imposed boundary conditions, the manifestation of the instability is plausibly enhanced with the increasing magnitude of the static, out-of-plane magnetic field. The enhancement is evident from a small magnetic perturbation of the governing equations of motion in our approach. This trend should persist even for larger magnetic fields within our model. It is tempting to expect that, if a DS-type instability is experimentally feasible in a 2D electronic fluid, it can be amplified by an applied static magnetic field. This hypothesis is open to further model refinements, and experimental verification.

The numerically observed gap between the stability ($\delta > 0$) and instability ($\delta < 0$) spectra, viewed as a *feature of a particular model* for the electronic fluid, may challenge the realization of a DS-type instability. This property suggests that there is no continuous passage from stability to instability through the variation of the Mach number within the shallow-water equations. Further scrutiny of this regime might require modification of the model. This task is not pursued in this paper.

2. Comparison of Cases I and II, and extraneous spectrum

Let us first review the stability formulation. Each of Cases I and II has a unique steady state. In Case I, the steady state yields lateral fluxes $\pm eBL\rho_0/(2m_e) = \pm\beta\rho_0 s_0/2$ (for $\breve{l} = 1$) at the left and right boundaries. As $\beta \to 0$, each steady state reduces to the DS case of constant density and normal flux, and zero tangential flux everywhere. We perturb the system around the steady states by linearizing the Euler equations with respective homogeneous boundary conditions; and compute the stability/instability spectra via eigenvalue problems. For $\beta \neq 0$ the spectra, and their sets of eigenmodes, are distinct for Cases I and II. In Case I, for all β the solution of the lateral-flux perturbation can *in principle* attain arbitrary nonzero yet mutually opposite values at the boundaries, which depend on the eigenmode. As $\beta \to 0$, the spectrum of Case I reduces to the union of the DS spectrum and a set of real frequencies, referred to as the extraneous spectrum; while Case II yields only the DS spectrum. In this nonmagnetic limit, for Case I the extraneous spectrum yields zero density and normal-flux perturbations whereas the remaining (DS) spectrum entails zero lateral-flux perturbation everywhere in the channel, as shown in Appendix D. The extraneous spectrum remains real valued if $\beta \neq 0$.

The superposition of eigenmodes for each case can express the unique solution of the *time dependent* system, Eq. (11), by linearization of the motion laws and imposition of suitable initial conditions under the same boundary conditions. Hence, the physically relevant eigenmodes and their contributions should be determined from the *initial preparation* of the system. For example, in Case I it is natural to expect and impose that, as $\beta \to 0$, the lateral-flux perturbation vanishes initially. The details of the time-dependent problem lie beyond our scope.

Let us now discuss the meaning of the extraneous spectrum (Case I). We reiterate two main features. First, this spectrum is real valued; thus, there is no growth (or decay) associated with it. Since the electron flow cannot be unstable at these frequencies, this response can hardly be viewed as a mechanism of generating THz electromagnetic radiation in the DS sense [23]. Second, in the limit $\beta \to 0$ the eigenmodes of the extraneous spectrum yield vanishing perturbations of density and normal flux, and a sinusoidal lateral-flux perturbation everywhere; see Appendix D. For an actual physical setting with $\beta = 0$, we can assume that the density and normal flux are *initially* perturbed around the steady state *nontrivially*, with nonzero values, while the lateral flux is zero. The imposition of such initial conditions would imply the elimination of the eigenmodes with real frequencies in the time-dependent linear response. By continuously perturbing this nonmagnetic setting with β, we can connect the ensuing time-dependent solution only to the complex, non-real-valued spectrum of Case I for $\beta \neq 0$. Thus, the extraneous spectrum becomes irrelevant.

VI. CONCLUSIONS

In this paper, we studied the effect of a static, out-of-plane magnetic field on the stability and instability spectra of a 2D inviscid electronic fluid in an infinitely long channel. Our model forms an extension of the Dyakonov-Shur model of plasma wave generation in 1D. We considered two cases of the boundary condition for the lateral flux. One of these cases (Case I)—with opposite lateral fluxes at the boundaries—is deemed as physically plausible. Another case (Case II)—with a zero lateral flux at the right boundary—is studied for comparison purposes. The main results of our study can be summarized as follows. First, we derived closed-form

analytical expressions for the respective spatially dependent steady state; and formulated eigenvalue problems by linear perturbations. Second, we demonstrated by numerics that the magnetic field enhances the growth exponents of the fluid instability. Third, we provided numerical evidence for the emergence of a magnetically controlled spectral gap.

Our study also indicates a subtlety inherent to the DS model. The DS spectrum may not always arise uniquely in the limit of a zero magnetic field in 2D. As an example, we showed that the imposition of mutually opposite boundary values of the lateral flux yields two distinct spectra, only one of which coincides with the DS prediction in each kinetic regime in the nonmagnetic limit. The other spectrum contains only real frequencies. This latter spectrum is deemed as irrelevant for our purpose, since it cannot induce an unstable electron flow.

Some open questions should be noted. In an actual 2D experimental setup, the channel has a finite length, say, L_y. This geometry breaks translation invariance in y, and requires suitable conditions at the top and bottom boundaries. For a broad family of such conditions, our results for the steady state would approximately hold away from the top and bottom boundaries if the channel is long enough, $L_y \gg L$. We expect that the lowest part of our computed spectrum would provide a good zeroth-order approximation if the length scale over which the fields of those modes vary, which is of the order of $|v_{x0} + s_0|/|\omega_n|$, is small compared to L_y. The combined effect of nonlinearities and magnetic field on the growth exponents has not been addressed. Finally, our prediction of a spectral gap could be the subject of laboratory testing, as well as the motivation for studying the validity or modification of the hydrodynamic model near the transition point.

ACKNOWLEDGMENTS

The authors are indebted to Prof. Andrew Lucas for bringing Ref. [23] and related published works to their attention, as well as for discussing physical aspects of the DS model with them. The authors also wish to thank Prof. Mitchell Luskin and Prof. Huy Q. Nguyen for useful discussions on the DS model; and an anonymous reviewer for suggesting the condition of mutually opposite boundary values of the tangential flux. The work of the first author (M.M.) was supported in part by the National Science Foundation Grants No. DMS-1912847, No. DMS-2045636, and by the Air Force Office of Scientific Research, USAF, under Grant/Contract No. FA9550-23-1-0007. The work of the second author (D.C.-R.) was supported by the NSF-REU via Grant No. DMS-2149913 at the University of Maryland. The third author (D.M.) is grateful to the School of Mathematics of the University of Minnesota for hosting him as an Ordway Distinguished Visitor, when part of this work was carried out.

APPENDIX A: STEADY-STATE SOLUTIONS FOR $\beta \neq 0$

In this Appendix, we derive the exact steady-state solutions of Sec. III B. We also extract small-$\beta\check{l}$ approximate formulas for the electronic number density.

1. Derivation of steady states for Cases I and II

Let us first address the case with mutually opposite lateral fluxes at the two boundaries, Case I. By using Eq. (11) with $(\partial/\partial t)(\check{\rho}, \check{v}_x, \check{v}_y) = 0$ and the notation $(\check{\rho}, \check{v}_x, \check{v}_y) = (\check{\rho}^s, \check{v}_x^s, \check{v}_y^s)$, we obtain

$$\left.\begin{aligned} \check{v}_x^s \tfrac{\partial \check{v}_x^s}{\partial \check{x}} + (2b)^{-1} \tfrac{\partial \check{\rho}^s}{\partial \check{x}} &= \beta(2b)^{-1} \check{v}_y^s, \\ \check{v}_x^s \tfrac{\partial \check{v}_y^s}{\partial \check{x}} &= -\beta \check{v}_x^s, \\ \tfrac{\partial}{\partial \check{x}}\left(\check{\rho}^s \check{v}_x^s\right) &= 0. \end{aligned}\right\} \tag{A1}$$

This is a system of ordinary differential equations (ODEs) subject to the conditions of Eq. (12). The last two ODEs are integrated directly, yielding (if $\check{v}_x^s \neq 0$)

$$\left.\begin{aligned} \check{v}_y^s &= \beta\left(\tfrac{\check{l}}{2} - \check{x}\right), \\ \check{\rho}^s \check{v}_x^s &= 1, \quad 0 \leqslant x \leqslant \check{l}. \end{aligned}\right\} \tag{A2}$$

Hence, by Eq. (A1) the Euler equation for $\check{v}_x^s$ reduces to

$$b\frac{\partial}{\partial \check{x}}\left(\check{v}_x^s\right)^2 + \frac{\partial \check{\rho}^s}{\partial \check{x}} = \beta^2\left(\frac{\check{l}}{2} - \check{x}\right), \quad 0 \leqslant \check{x} \leqslant \check{l}.$$

This equation is integrated by application of the condition $\check{\rho}^s = 1$ at $\check{x} = 0$, and furnishes

$$\check{\rho}^s - 1 + b\left[\left(\check{v}_x^s\right)^2 - 1\right] = \frac{\beta^2}{2}\check{x}(\check{l} - \check{x}), \quad 0 \leqslant \check{x} \leqslant \check{l}.$$

Recalling that $\check{\rho}^s \check{v}_x^s = 1$, we find the cubic equation

$$\zeta^3 - \zeta^2 + \epsilon^2 = 0, \tag{A3}$$

where $\zeta = [1 + b + (\beta^2/2)\check{x}(\check{l} - \check{x})]^{-1}\check{\rho}^s$ and

$$\epsilon^2 = \frac{b}{\left[1 + b + \frac{\beta^2}{2}\check{x}(\check{l} - \check{x})\right]^3}. \tag{A4}$$

Note that $b(1 + b + \beta^2\check{l}^2/8)^{-3} \leqslant \epsilon(\check{x})^2 \leqslant b(1 + b)^{-3}$ for $0 \leqslant \check{x} \leqslant \check{l}$, which precisely describes the minimum and the maximum value of $\epsilon(\check{x})^2$ in the channel. The maximum value in $\check{x}$ is attained if we let $\check{x} = 0$ or $\check{x} = \check{l}$, and (as a function of b) is maximized, becoming equal to $4/27$, for $b = 1/2$. By writing Eq. (A3) as $\epsilon^2 = \zeta^2(1 - \zeta)$, we notice that any physically admissible solution, $\zeta = \zeta^s$, must satisfy $0 < \zeta^s \leqslant 1$ for $b > 0$. The value $\zeta^s = (1 + b)^{-1}$ is an admissible root for $\epsilon^2 = b(1 + b)^{-3}$, which corresponds to the boundary condition for $\check{\rho}^s$ at $\check{x} = 0$ and gives the same value at $\check{x} = \check{l}$.

Next, we solve Eq. (A3) by the known procedure based on Vieta's substitution [34,35]. This equation is of the form $\zeta^3 + a_2\zeta^2 + a_1\zeta + a_0 = 0$ with $a_2 = -1$, $a_1 = 0$ and $a_0 = \epsilon^2$. Accordingly, following [35] we define

$$q = \frac{1}{3}a_1 - \frac{1}{9}a_2^2 = -\frac{1}{9},$$
$$p = \frac{1}{6}(a_1 a_2 - 3a_0) - \frac{1}{27}a_2^3 = -\frac{\epsilon^2}{2} + \frac{1}{27}.$$

The sign of the quantity $q^3 + p^2$ determines how many real roots the cubic equation has. We compute

$$q^3 + p^2 = \frac{\epsilon^2}{4}\left(\epsilon^2 - \frac{4}{27}\right) \leqslant 0.$$

Hence, all roots of Eq. (A3) are real [34,35]. Now define

$$\varsigma_\pm = [p \pm (q^3 + p^2)^{1/2}]^{1/3},$$

with the typical convention that $\mathrm{Im}\,(q^3 + p^2)^{1/2} \geqslant 0$. The root of interest is written as

$$\zeta^s = \varsigma_+ + \varsigma_- - \frac{a_2}{3} = \frac{1}{3} + \sum_{s=\pm 1} \left(\frac{1}{27} - \frac{\epsilon^2}{2} + \mathrm{i}\, s \frac{\epsilon}{2} \sqrt{\frac{4}{27} - \epsilon^2} \right)^{1/3}. \quad \text{(A5)}$$

This root is the only physically admissible one. For example, it reduces to the solution of the nonmagnetic case, as $B \to 0$ [23]. We omit the details of this limit here.

To simplify the above expression for ζ^s, we use the following identity, for all real ϵ with $|\epsilon| \leqslant \frac{2}{3\sqrt{3}}$:

$$\left| \frac{1}{27} - \frac{\epsilon^2}{2} \pm \mathrm{i} \frac{\epsilon}{2} \sqrt{\frac{4}{27} - \epsilon^2} \right| = \frac{1}{27},$$

by which we set

$$\frac{1}{27} - \frac{\epsilon^2}{2} \pm \mathrm{i} \frac{\epsilon}{2} \sqrt{\frac{4}{27} - \epsilon^2} = \frac{1}{27} e^{\pm \mathrm{i}\theta}, \quad 0 \leqslant \theta \leqslant 2\pi.$$

Thus, we obtain the anticipated formula

$$\zeta^s = \frac{2}{3} \cos\left(\frac{\theta}{3}\right) + \frac{1}{3}, \quad \text{(A6)}$$

where

$$\cos\theta = 1 - \frac{27}{2}\epsilon^2. \quad \text{(A7)}$$

This equation must be inverted for θ in view of Eq. (A6). Thus, θ is given in terms of some *generalized* inverse cosine, a multivalued function, with argument $1 - (27/2)\epsilon^2$, which must be evaluated by appropriate analytic continuation in ϵ^2 as $\check{x}$ and b vary. Once ζ^s is determined in this way, we have

$$\check{\rho}^s = [1 + b + (\beta^2/2)\check{x}(\check{l} - \check{x})] \left[\frac{2}{3} \cos\left(\frac{\theta}{3}\right) + \frac{1}{3} \right] \quad \text{(A8)}$$

and $\check{v}_x^s = 1/\check{\rho}^s$ for all $\check{x}$ $(0 \leqslant \check{x} \leqslant \check{l})$.

We should outline the implications from the multivaluedness that is inherent to the generalized inverse cosine function, as ϵ^2 varies through the change of b and $\check{x}$ $(0 \leqslant \check{x} \leqslant \check{l})$. For definiteness, we invoke the principal branch of $\cos^{-1}(\cdot)$, defined by

$$0 \leqslant \cos^{-1} z \leqslant \pi, \quad \text{if } -1 \leqslant z \leqslant 1.$$

From now on, the symbol $\cos^{-1} z$ denotes a real single-valued function under the above definition.

First, consider the solution with

$$\theta(\check{x}; b) = \cos^{-1}\left(1 - \tfrac{27}{2}\epsilon(\check{x}; b)^2\right), \quad \text{(A9)}$$

which entails $2/3 < \zeta^s \leqslant 1$ by virtue of Eq. (A6). The boundary condition at $\check{x} = 0$ reads as $\zeta^s = (1 + b)^{-1}$, and is manifest in this particular branch only if

$$0 \leqslant b < 1/2,$$

which signifies the subsonic regime. For this range of b, if $\check{x}$ increases continuously from 0 to $\check{l}$ the quantity $1 - (27/2)\epsilon(\check{x})^2$ increases continuously taking values in an interval contained entirely in $[-1, 1]$. We thus verify (self consistently) that in this kinetic regime $\theta(\check{x}; b)$ remains in the same branch for the whole channel up to the boundaries, $0 \leqslant \check{x} \leqslant \check{l}$.

On the other hand, consider the solution with

$$\theta(\check{x}; b) = 2\pi - \cos^{-1}\left(1 - \tfrac{27}{2}\epsilon(\check{x}; b)^2\right), \quad \text{(A10)}$$

which corresponds to a different branch of the underlying generalized inverse cosine and entails $0 \leqslant \zeta^s < 2/3$. Accordingly, the enforcement of the boundary condition at $\check{x} = 0$ is equivalent to the restriction

$$b > 1/2,$$

which characterizes the supersonic regime. As $\check{x}$ continuously increases from 0 to $\check{l}$ inside the channel, we verify that the function $\theta(\check{x}; b)$ lies in this particular branch.

Hence, for fixed $\check{x}$ $(\check{x} \neq 0, \check{l})$ and nonzero β, we can show that the continuous variation of b from values $b < 1/2$ to $b > 1/2$, through the transition point, reveals a jump discontinuity of the electronic number density (as a function of b) at $b = 1/2$. The jump disappears in the limit of zero magnetic field $(\beta \to 0)$, when the density approaches a constant everywhere in the channel [23].

Let us now discuss the case with a vanishing lateral flux at the right boundary, Case II. We need to solve Eq. (A1) subject to the conditions of Eq. (13). We obtain

$$\left.\begin{aligned} \check{v}_y^s &= \beta(\check{l} - \check{x}), \\ \check{\rho}^s\, \check{v}_x^s &= 1, \quad 0 \leqslant x \leqslant \check{l}. \end{aligned}\right\} \quad \text{(A11)}$$

Thus, the Euler equation for $\check{v}_x^s$ becomes

$$b \frac{\partial}{\partial \check{x}} (\check{v}_x^s)^2 + \frac{\partial \check{\rho}^s}{\partial \check{x}} = \beta^2(\check{l} - \check{x}), \quad 0 \leqslant \check{x} \leqslant \check{l}.$$

We find Eq. (A3) with $\zeta = [1 + b + (\beta^2/2)\check{x}(2\check{l} - \check{x})]^{-1} \check{\rho}^s$ and

$$\epsilon^2 = \frac{b}{\left[1 + b + \frac{\beta^2}{2}\check{x}(2\check{l} - \check{x})\right]^3}. \quad \text{(A12)}$$

Note that $b(1 + b + \beta^2\check{l}^2/2)^{-3} \leqslant \epsilon(\check{x})^2 \leqslant b(1 + b)^{-3}$, where the maximum value of $\epsilon(\check{x})^2$ is attained at $\check{x} = 0$. Without further ado, we recover formula (A8) with the replacement of the factor $\check{x}(\check{x} - \check{l})$ by $\check{x}(2\check{l} - \check{x})$. The function $\theta(\check{x}; b)$ is defined by Eq. (A9) if $0 \leqslant b < 1/2$, or Eq. (A10) if $b > 1/2$ in view of Eq. (A12). Thus, the branching described in Case I above persists here as well.

2. Small-$\beta\check{l}$ perturbations

Next, we simplify formula (A8) when the magnetic field is sufficiently weak, focusing on Case I, with mutually opposite lateral fluxes at the boundaries. For fixed $b \neq \frac{1}{2}$, the density $\check{\rho}^s$ is controlled by the parameter $\epsilon(\check{x})^2$. By Eq. (A4), we notice that ϵ^2 varies spatially according to the term $\frac{\beta^2}{2}\check{x}(\check{l} - \check{x})$, which is positive and less than or equal to $\mathcal{O}((\beta\check{l})^2)$ if $0 < \check{x} < \check{l}$. Thus, the relevant parameter is $\beta\check{l}$. We enforce the condition $|\beta|\check{l} \ll 1$.

First, let us apply regular perturbations in β. To reduce the algebra, we write the cubic equation for $\breve{\rho}^s$ as

$$1-\breve{\rho}^s=\frac{\beta^2}{2}\breve{x}(\breve{l}-\breve{x})\frac{(\breve{\rho}^s)^2}{b(1+\breve{\rho}^s)-(\breve{\rho}^s)^2}.$$

The right-hand side of this equation is small if b is away from the transition point. In this case, an expansion for $\breve{\rho}^s$ can be obtained by iterations with the zeroth-order solution $\breve{\rho}^s=1$. The first iteration gives

$$1-\breve{\rho}^s=-\frac{\beta^2}{2(1-2b)}\breve{x}(\breve{l}-\breve{x})+\mathcal{O}\big((\beta\breve{l})^4\big),$$

which entails Eq. (19a). This expansion is meaningful if

$$\frac{\beta^2}{2(1-2b)}\breve{x}(\breve{l}-\breve{x})\ll 1.$$

Thus, we must have $(\beta\breve{l})^2\ll|1-2b|$.

When $(\beta\breve{l})^2=\mathcal{O}(|1-2b|)$, the above regular expansion for $\breve{\rho}^s$ breaks down. In this case, b is near $1/2$. Define the small parameters

$$\delta=b-\frac{1}{2},\quad \varepsilon=\frac{\beta^2}{2}\breve{x}(\breve{l}-\breve{x}). \tag{A13}$$

We are interested in the regime with $\varepsilon\leqslant\mathcal{O}(\delta)$. Let $\breve{\rho}^s=1+\varrho_c$. The correction term ϱ_c satisfies

$$-2(\delta+\varepsilon)\varrho_c+\left[\tfrac{3}{2}-(\delta+\varepsilon)\right]\varrho_c^2+\varrho_c^3=\varepsilon.$$

For the critical scaling of interest, we set $\delta+\varepsilon=\alpha\delta$ for some $\alpha=\mathcal{O}(1)$. By dominant balance, we find

$$\varrho_c^2\simeq\frac{2\varepsilon}{3}\ \Rightarrow\ \varrho_c\simeq\pm\sqrt{\frac{2\varepsilon}{3}}.$$

By Eq. (A8) for $\theta\simeq\pi$ and $(\beta\breve{l})^2\ll 1$, we assert that $\breve{\rho}^s-1>0$ for $b<1/2$ (if $\theta<\pi$) and $\breve{\rho}^s-1<0$ for $b>1/2$ ($\theta>\pi$) near the transition point ($b\simeq 1/2$). Thus, we must set $\pm=\mathrm{sgn}(1-2b)$ in the approximate formula for ϱ_c. This substitution yields Eq. (19b).

Alternatively, consider Case II, with the boundary condition of a vanishing lateral flux at $\breve{x}=\breve{l}$. Evidently, the above procedure remains essentially intact, yet with the replacement of the expression for ε in Eq. (A13) by $\varepsilon=\frac{\beta^2}{2}\breve{x}(2\breve{l}-\breve{x})$. Thus, the factor $\breve{x}(\breve{l}-\breve{x})$ is replaced by $\breve{x}(2\breve{l}-\breve{x})$.

APPENDIX B: ON THE LINEAR STABILITY PROBLEM

In this Appendix, we provide details on the linear stability formulation of Sec. IV. Our primary hydrodynamic variables are the rescaled density $\breve{\rho}$ and vector-valued flux $(\breve{J}_x,\breve{J}_y)=(\breve{\rho}\breve{v}_x,\breve{\rho}\breve{v}_y)$.

Consider the y-independent governing motion laws of Eq. (11). By multiplying the first (second) equation by $\breve{\rho}$ and the third equation by $\breve{v}_x$ ($\breve{v}_y$) and then adding the respective two equations together, we obtain the system

$$\frac{\partial\breve{J}_x}{\partial\breve{t}}+\frac{\partial}{\partial\breve{x}}\left(\frac{\breve{J}_x^2}{\breve{\rho}}\right)=(2b)^{-1}\left(-\frac{1}{2}\frac{\partial\breve{\rho}^2}{\partial\breve{x}}+\beta\breve{J}_y\right), \tag{B1}$$

$$\frac{\partial\breve{J}_y}{\partial\breve{t}}+\frac{\partial}{\partial\breve{x}}\left(\frac{\breve{J}_x\breve{J}_y}{\breve{\rho}}\right)=-\beta\breve{J}_x, \tag{B2}$$

$$\frac{\partial\breve{\rho}}{\partial\breve{t}}+\frac{\partial\breve{J}_x}{\partial\breve{x}}=0. \tag{B3}$$

We also impose one of two sets of boundary conditions. For Case I, one such set comes from Eq. (12), viz.,

$$\breve{\rho}=1\quad\text{at }\breve{x}=0, \tag{B4}$$

$$\breve{J}_x=1\quad\text{at }\breve{x}=\breve{l}, \tag{B5}$$

$$\breve{J}_y\big|_{\breve{x}=0}+\breve{J}_y\big|_{\breve{x}=\breve{l}}=0. \tag{B6}$$

For Case II, the boundary conditions are described by Eq. (13), which amounts to Eqs. (B4) and (B5) with

$$\breve{J}_y=0\quad\text{at }\breve{x}=\breve{l}. \tag{B7}$$

Next, we perturb the governing equations around the steady-state solution $(\breve{J}_x^s,\breve{J}_y^s,\breve{\rho}^s)$, writing

$$(\breve{J}_x,\breve{J}_y)=\big(\breve{J}_x^s(\breve{x}),\breve{J}_y^s(\breve{x})\big)+(\breve{\jmath}_1(\breve{x}),\breve{\jmath}_2(\breve{x}))e^{-\breve{\Lambda}\breve{t}},$$

$$\breve{\rho}=\breve{\rho}^s(\breve{x})+\breve{\rho}_1(\breve{x})e^{-\breve{\Lambda}\breve{t}},\quad\text{for }0<\breve{x}<\breve{l}.$$

Our purpose now is to linearize the governing equations for the perturbation $(\breve{\jmath}_1,\breve{\jmath}_2,\breve{\rho}_1)$. This step is illustrated by the following successive approximations:

$$\begin{aligned}
\big(\breve{J}_x^s+\breve{\jmath}_1e^{-\breve{\Lambda}\breve{t}}\big)^2&\simeq\big(\breve{J}_x^s\big)^2+2\breve{J}_x^s\,\breve{\jmath}_1e^{-\breve{\Lambda}\breve{t}},\ (\breve{\rho}^s+\breve{\rho}_1e^{-\breve{\Lambda}\breve{t}})^{-1}\simeq(\breve{\rho}^s)^{-1}\left(1-\frac{\breve{\rho}_1}{\breve{\rho}^s}e^{-\breve{\Lambda}\breve{t}}\right),\\
&\times\big(\breve{J}_x^s+\breve{\jmath}_1e^{-\breve{\Lambda}\breve{t}}\big)^2(\breve{\rho}^s+\breve{\rho}_1e^{-\breve{\Lambda}\breve{t}})^{-1}\simeq(\breve{\rho}^s)^{-1}\\
&\times\left\{\big(\breve{J}_x^s\big)^2+\breve{J}_x^s\left(2\breve{\jmath}_1-\breve{J}_x^s\frac{\breve{\rho}_1}{\breve{\rho}^s}\right)e^{-\breve{\Lambda}\breve{t}}\right\},\ (\breve{\rho}^s+\breve{\rho}_1e^{-\breve{\Lambda}\breve{t}})^2\simeq(\breve{\rho}^s)^2+2\breve{\rho}^s\,\breve{\rho}_1\,e^{-\breve{\Lambda}\breve{t}},\\
&\times\big(\breve{J}_x^s+\breve{\jmath}_1e^{-\breve{\Lambda}\breve{t}}\big)\big(\breve{J}_y^s+\breve{\jmath}_2e^{-\breve{\Lambda}\breve{t}}\big)\simeq\breve{J}_x^s\breve{J}_y^s+\big(\breve{\jmath}_1\breve{J}_y^s+\breve{\jmath}_2\breve{J}_x^s\big)e^{-\breve{\Lambda}\breve{t}},\\
&\times(\breve{\rho}^s+\breve{\rho}_1e^{-\breve{\Lambda}\breve{t}})^{-1}\big(\breve{J}_x^s+\breve{\jmath}_1e^{-\breve{\Lambda}\breve{t}}\big)\big(\breve{J}_y^s+\breve{\jmath}_2e^{-\breve{\Lambda}\breve{t}}\big)\\
&\simeq(\breve{\rho}^s)^{-1}\left\{\breve{J}_x^s\breve{J}_y^s+\left(\breve{\jmath}_1\breve{J}_y^s+\breve{\jmath}_2\breve{J}_x^s-\breve{J}_x^s\breve{J}_y^s\frac{\breve{\rho}_1}{\breve{\rho}^s}\right)e^{-\breve{\Lambda}\breve{t}}\right\}.
\end{aligned}$$

The simplification of the nonlinear terms in Eqs. (B1)–(B3) by virtue of these approximate expressions and further manipulations yield Eq. (20) for $\check{\Lambda} = \mathrm{i}\check{\omega}$. The homogeneous boundary conditions of Eq. (21) or (22) for $(\check{\jmath}_1, \check{\jmath}_2, \check{\rho}_1)$ follow from the fact that the steady-state solution $(\check{J}_x^s, \check{J}_y^s, \check{\rho}^s)$ satisfies boundary conditions (B4) and (B5) with Eq. (B6) or (B7).

APPENDIX C: NUMERICAL APPROACH

In this Appendix, we outline our numerical approach for solving the eigenvalue problems of Cases I and II. The algorithms have been implemented in the Julia programming language [36].

1. Finite-difference approximation

We discretize the operator of Eq. (20) with a central difference quotient under elliptic regularization. For a given number N of subintervals of $[0, \check{l}]$, for the finite-difference approximation we set $\check{x}_i = \check{h}\, i$ for $i = 0, ...N$, where $\check{h} = \check{l}/N$. We also introduce finite-difference stencils approximating the first and second derivatives of an arbitrary discrete function $f(\check{x}_i)$ as follows:

$$\delta_{\check{h}} f_i = \frac{f_{i+1} - f_{i-1}}{2\check{h}},\ \delta^+_{\check{h}} f_i = \frac{f_{i+1} - f_i}{\check{h}},\ \delta^-_{\check{h}} f_i = \frac{f_i - f_{i-1}}{\check{h}},$$
$$\Delta_{\check{h}} f_i = \frac{f_{i+1} - 2f_i + f_{i-1}}{\check{h}^2}.$$

Here, we employ the short notation $f_i := f(\check{x}_i)$. Note that the central-difference stencils $\delta_{\check{h}} f_i$ and $\Delta_{\check{h}} f_i$ are second-order approximations of the first and second derivative of f, whereas $\delta^+_{\check{h}} f$ and $\delta^-_{\check{h}} f$ lead to first-order approximations. Let $\mathbb{C}$ denote the set of all complex numbers. The desired discrete eigenvalue problem then reads as follows: Find a nontrivial $\overline{U}^{\check{h}} \in \mathbb{C}^{N+1}$ and $\check{\omega}^{\check{h}} \in \mathbb{C}$ such that for $i = 1, \ldots, N-1$ we have

$$\check{h}^2 c\, \Delta_{\check{h}} \overline{U}^{\check{h}}_i \ + \ \delta_{\check{h}} \{ \mathbb{A}(\check{x}_i) \overline{U}^{\check{h}}_i \} \ + \ \beta \mathbb{B}\, \overline{U}^{\check{h}}_i \ = \ \mathrm{i}\, \check{\omega}^{\check{h}}\, \overline{U}^{\check{h}}_i.$$

The factor $c \in \{-1, 1\}$ is set to 1 for approximating the subsonic spectrum ($\delta < 0$) and to -1 for the supersonic spectrum ($\delta > 0$); thus, $c = -\mathrm{sgn}(\delta)$ where sgn is the signum function. The system is supplemented with three additional difference equations on the left and right boundaries where we have to take a one-sided difference operator: We introduce two equations with forward-difference stencil for the first two components ($k = 1, 2$) at $\check{x}_0$, the left boundary; and one equation with backward-difference stencil for the last component ($k = 3$) at $\check{x}_N$, the right boundary. These equations read

$$\delta^+_{\check{h}} \{ (\mathbb{A}(\check{x}_0) \overline{U}^{\check{h}}_0)_k \} + \beta (\mathbb{B}\, \overline{U}^{\check{h}}_0)_k = \mathrm{i}\, \check{\omega}^{\check{h}}\, (\overline{U}^{\check{h}}_0)_k,$$
$$\delta^-_{\check{h}} \{ (\mathbb{A}(\check{x}_N) \overline{U}^{\check{h}}_N)_k \} + \beta (\mathbb{B}\, \overline{U}^{\check{h}}_N)_3 = \mathrm{i}\, \check{\omega}^{\check{h}}\, (\overline{U}^{\check{h}}_N)_3.$$

Note that for each component we enforce the equation with a one-sided difference operator on the *opposite side* to the boundary where we have to enforce a corresponding Dirichlet boundary condition on the component.

Finally, to apply the requisite boundary conditions, we complete the linear system by imposing three additional equations. Two of these equations are

$$42^2 (\overline{U}^{\check{h}}_N)_1 = \mathrm{i}\, \check{\omega}^{\check{h}} (\overline{U}^{\check{h}}_N)_1, \quad 42^2 (\overline{U}^{\check{h}}_0)_3 = \mathrm{i}\, \check{\omega}^{\check{h}} (\overline{U}^{\check{h}}_0)_3.$$

Furthermore, depending on whether we enforce Eq. (21) or (22) for the tangential flux, under Case I or II, respectively, we impose one of the following equations:

$$\text{Case I:} \quad \frac{42^2}{\check{h}^2} (\overline{U}^{\check{h}}_0 + \overline{U}^{\check{h}}_N)_2 \ = \ \mathrm{i}\, \check{\omega}^{\check{h}} (\overline{U}^{\check{h}}_N)_2,$$
$$\text{Case II:} \quad 42^2 (\overline{U}^{\check{h}}_N)_2 \ = \ \mathrm{i}\, \check{\omega}^{\check{h}} (\overline{U}^{\check{h}}_N)_2.$$

The numerical value 42^2 shown above is guaranteed not to coincide with any of the eigenfrequencies $\check{\omega}^{\check{h}}$. For Case I, this scheme implies that

$$\overline{U}^{\check{h}}_0 + \overline{U}^{\check{h}}_N = 0 + \mathcal{O}(h^2).$$

Correspondingly, for Case II we have $\overline{U}^{\check{h}}_N = 0$.

We can now collect all equations into a *stiffness matrix* $\mathbb{S}$ where $\mathbb{S} \in \mathbb{R}^{(N+1)\times(N+1)}$. The final system of linear equations thus reads

$$\mathbb{S}_{\check{h}} \overline{U}^{\check{h}} \ = \ \mathrm{i}\, \check{\omega}^{\check{h}}\, \overline{U}^{\check{h}}. \tag{C1}$$

2. Implementation and Richardson extrapolation

The discrete eigenvalue problem described by Eq. (C1) is implemented in the *Julia* programming language. Because of the fact that Eq. (C1) expresses a nonsymmetric eigenvalue problem of modest size, we have opted to apply Julia's `eigen()` function, which internally uses `LAPACK` routines for computing the spectrum and eigenvectors. This approach is reasonably efficient for problem sizes up to $N \leqslant 2500$, which is our target resolution. A possible alternative suitable for larger systems would have been a *Krylov subspace method* such as the Krylov-Schur algorithm.

We have verified numerically that we are indeed in an *asymptotic regime* for increasing degree of resolution with $N = 320$, 640, 1280, and 2560. This means that the observed numerical error decreases with N with a convergence order of 2. In order to minimize the error, we have opted to perform a single step of a *Richardson extrapolation*, exploiting the fact that we are in an asymptotic regime. In this vein, we first compute the spectrum for $N = 1280$ and $N = 2560$. Then, we filter the spectrum to relevant eigenfrequencies and identify all corresponding eigenfrequencies $(\check{\omega}^{\check{h}}_n, \check{\omega}^{\check{h}/2}_n)$ between the two sets, and extrapolate as follows:

$$\check{\omega}^{\mathrm{extr.}}_n \ = \ \frac{\check{\omega}^{\check{h}/2}_n - 2^{-2} \check{\omega}^{\check{h}}_n}{1 - 2^{-2}}.$$

The resulting numerical value $\check{\omega}^{\mathrm{extr.}}_n$ is fourth-order convergent. We estimate the final relative discretization error to be less than 2%.

APPENDIX D: ON LIMIT OF FLUID SPECTRUM AS $\beta \to 0$

In this Appendix, we study the limit of the fluid spectrum as the magnetic field tends to zero. We examine Cases I and II separately.

Consider Eq. (20). The coefficients of this system are well behaved for sufficiently small $|\boldsymbol{B}|$. Hence, we can obtain the limit of the solution $(\overline{U}(\check{x}), \check{\omega})$ as $\beta \to 0$ by setting $\beta = 0$ in Eq. (20). The resulting system reads

$$\mathbb{A}^0 \frac{\partial}{\partial \check{x}} \overline{U}^{(0)}(\check{x}) \;=\; \mathrm{i}\,\check{\omega}^0\, \overline{U}^{(0)}(\check{x}), \tag{D1}$$

where $\overline{U}^{(0)} = (\check{\jmath}_1^0, \check{\jmath}_2^0, \check{\rho}_1^0)^T$ and

$$\mathbb{A}^0 = \begin{pmatrix} 2 & 0 & \frac{1-2b}{2b} \\ 0 & 1 & 0 \\ 1 & 0 & 0 \end{pmatrix}.$$

We seek nontrivial solutions $(\overline{U}^{(0)}, \check{\omega}^0)$ under Eq. (21) for Case I; or, alternatively, Eq. (22) for Case II.

The eigenvalues of matrix $\mathbb{A}^0$ are $\lambda_0 = 1$ and $\lambda_\pm = 1 \pm (2b)^{-1/2}$. The corresponding eigenvectors are generated from $\overline{U}_0^{(0)} = (0, \lambda_0, 0)^T$ and $\overline{U}_\pm^{(0)} = (\lambda_\pm, 0, 1)^T$. Hence, the general nontrivial solution to Eq. (D1) reads

$$\overline{U}^{(0)}(\check{x}) = \sum_{p=0,\pm} C_p e^{\mathrm{i}(\check{\omega}^0/\lambda_p)\check{x}}\, \overline{U}_p^{(0)}, \tag{D2}$$

where C_p $(p = 0, \pm)$ is an arbitrary complex number with $(C_0, C_+, C_-) \neq (0, 0, 0)$. This formulation yields

$$\check{\jmath}_1^0(\check{x}) = \sum_{p=\pm} C_p \lambda_p e^{\mathrm{i}\frac{\check{\omega}^0}{\lambda_p}\check{x}}, \tag{D3}$$

$$\check{\jmath}_2^0(\check{x}) = C_0 e^{i\frac{\check{\omega}^0}{\lambda_0}\check{x}}, \tag{D4}$$

$$\check{\rho}_1^0(\check{x}) = \sum_{p=\pm} C_p e^{\mathrm{i}\frac{\check{\omega}^0}{\lambda_p}\check{x}}, \quad 0 \leqslant \check{x} \leqslant \check{l}. \tag{D5}$$

The eigenfrequencies $\check{\omega}^0$ must now be determined by imposition of the boundary conditions. Note the linear independence of the lateral-flux field from the other two scalar fields.

1. Zero lateral flux at the right boundary (Case II)

We apply Eq. (22). Consequently, by $\check{\jmath}_2^0(\check{l}) = 0$ we obtain $C_0 = 0$ for any $\check{\omega}^0$. This in turn implies that $\check{\jmath}_2^0(\check{x})$ *vanishes everywhere*. The constants $C_\pm$ satisfy

$$\left.\begin{aligned} C_+ + C_- &= 0, \\ C_+\lambda_+ e^{\mathrm{i}\frac{\check{\omega}^0}{\lambda_+}\check{l}} + C_-\lambda_- e^{\mathrm{i}\frac{\check{\omega}^0}{\lambda_-}\check{l}} &= 0. \end{aligned}\right\} \tag{D6}$$

By virtue of $(C_+, C_-) \neq (0, 0)$, we derive the whole DS spectrum for $\check{\omega}^0$, Eq. (4a). Thus, in this case the DS predictions are uniquely recovered as $\beta \to 0$ in our model. The normal flux and number density are nontrivial.

2. Opposite lateral fluxes at boundaries (Case I)

Let us now apply Eq. (21), which includes the condition $\check{\jmath}_2^0(0) = -\check{\jmath}_2^0(\check{l})$. Accordingly, we obtain

$$C_0 \cos\left(\tfrac{\check{\omega}^0\check{l}}{2}\right) = 0. \tag{D7}$$

In addition, Eq. (D6) must hold. Thus, we need to distinguish two cases for C_0 (and $\check{\omega}^0$). First, if $C_0 = 0$ then we obtain the DS solution with the familiar DS spectrum and nonzero normal flux and number density.

On the other hand, if $C_0 \neq 0$, we find

$$\check{\omega}_n^0 = (2n+1)\frac{\pi}{\check{l}} \quad (n \in \mathbb{Z}) \tag{D8}$$

and

$$\check{\jmath}_2^0(\check{x}) = C_0 e^{\mathrm{i}(2n+1)\frac{\pi}{\check{l}}\check{x}}, \quad 0 \leqslant \check{x} \leqslant \check{l}. \tag{D9}$$

Accordingly, we assert that $C_+ = C_- = 0$, which yields *zero density and normal flux everywhere*. In conclusion, in Case I the total fluid spectrum consists of the DS spectrum and the extraneous set of real-valued eigenfrequencies from Eq. (D8).

[1] M. Tonouchi, Cutting-edge terahertz technology, Nat. Photonics **1**, 97 (2007).

[2] G. K. Kitaeva, Terahertz radiation by means of optical lasers, Laser Phys. Lett. **5**, 559 (2008).

[3] D. S. Rana and M. Tonouchi, Terahertz emission functionality of high-temperature superconductors and similar complex systems, Adv. Opt. Mater. **8**, 1900892 (2020).

[4] S. S. Dhillon, M. S. Vitiello, E. H. Linfield, A. G. Davies, M. C. Hoffmann, J. Booske, C. Paoloni, M. Gensch, P. Weightman, G. P. Williams *et al.*, The 2017 terahertz science and technology roadmap, J. Phys. D: Appl. Phys. **50**, 043001 (2017).

[5] K. Sengupta, T. Nagatsuma, and D. M. Mittleman, Terahertz integrated electronic and hybrid electronic-photonic systems, Nat. Electron. **1**, 622 (2018).

[6] J. A. Fülöp, S. Tzortzakis, and T. Kampfrath, Laser-driven strong-field terahertz sources, Adv. Opt. Mater. **8**, 1900681 (2020).

[7] W. L. Chan, J. Deibel, and D. M. Mittleman, Imaging with terahertz radiation, Rep. Prog. Phys. **70**, 1325 (2007).

[8] D. L. Woolard, R. Broan, M. Pepper, and M. Kemp, Terahertz frequency sensing and imaging: A time of reckoning future applications? Proc. IEEE **93**, 1722 (2005).

[9] T. Hattori and M. Sakamoto, Deformation corrected real-time terahertz imaging, Appl. Phys. Lett. **90**, 261106 (2007).

[10] E. Knoesel, M. Bonn, J. Shan, and T. F. Heinz, Charge transport and carrier dynamics in liquids probed by THz time-domain spectroscopy, Phys. Rev. Lett. **86**, 340 (2001).

[11] D. S. Rana, K. Takahashi, K. R. Mavani, I. Kawayama, H. Murakami, and M. Tonouchi, Visualization of photoassisted polarization switching and its consequences in $BiFeO_3$ thin films probed by terahertz radiation, Appl. Phys. Lett. **91**, 031909 (2007).

[12] C. P. Hauri, C. Ruchert, C. Vicario, and F. Ardana, Strong-field single-cycle THz pulses generated in an organic crystal, Appl. Phys. Lett. **99**, 161116 (2011).

[13] L. E. F. Foa Torres, S. Roche, and J.-C. Charlier, *Introduction to Graphene-Based Nanomaterials: From Electronic Structure to Quantum Transport* (Cambridge University Press, Cambridge, 2014).

[14] A. K. Geim and I. V. Grigorieva, van der Waals heterostructures, Nature (London) **499**, 419 (2013).

[15] A. H. Castro Neto, F. Guinea, N. M. R. Peres, K. S. Novoselov, and A. K. Geim, The electronic properties of graphene, Rev. Mod. Phys. **81**, 109 (2009).

[16] K. S. Novoselov, V. I. Fal'ko, L. Colombo, P. R. Gellert, M. G. Schwab, and K. Kim, A roadmap for graphene, Nature (London) **490**, 192 (2012).

[17] R. N. Gurzhi, Hydrodynamic effects in solids at low temperature, Sov. Phys. Usp. **11**, 255 (1968).

[18] A. Lucas and K. C. Fong, Hydrodynamics of electrons in graphene, J. Phys.: Condens. Matter **30**, 053001 (2018).

[19] D. A. Bandurin, I. Torre, R. K. Kumar, M. B. Shalom, A. Tomadin, A. Principi, G. H. Auton, E. Khestanova, K. S. Novoselov, I. V. Grigorieva *et al.*, Negative local resistance caused by viscous electron backflow in graphene, Science **351**, 1055 (2016).

[20] J. Crossno, J. K. Shi, K. Wang, X. Liu, A. Harzheim, A. Lucas, S. Sachdev, P. Kim, T. Taniguchi, K. Watanabe *et al.*, Observation of the Dirac fluid and the breakdown of the Wiedemann-Franz law in graphene, Science **351**, 1058 (2016).

[21] R. K. Kumar, D. A. Bandurin, F. M. D. Pellegrino, Y. Cao, A. Principi, H. Guo, G. H. Auton, M. B. Shalom, L. A. Ponomarenko, G. Falkovich *et al.*, Superballistic flow of viscous electron fluid through graphene constrictions, Nat. Phys. **13**, 1182 (2017).

[22] D. A. Bandurin, A. V. Shytov, L. S. Levitov, R. K. Kumar, A. I. Berdyugin, M. Ben Shalom, I. V. Grigorieva, A. K. Geim, and G. Falkovich, Fluidity onset in graphene, Nat. Commun. **9**, 4533 (2018).

[23] M. Dyakonov and M. Shur, Shallow water analogy for a ballistic field effect transistor: New mechanism of plasma wave generation by dc current, Phys. Rev. Lett. **71**, 2465 (1993).

[24] C. B. Mendl, M. Polini, and A. Lucas, Coherent terahertz radiation from a nonlinear oscillator of viscous electrons, Appl. Phys. Lett. **118**, 013105 (2021).

[25] J. Crabb, X. Cantos-Roman, G. R. Aizin, and J. M. Jornet, Amplitude and frequency modulation with an on-chip graphene-based plasmonic terahertz nanogenerator, IEEE Trans. Nanotechnol. **21**, 539 (2022).

[26] S. Bhardwaj, N. K. Nahar, S. Rajan, and J. L. Volakis, Numerical analysis of terahertz emissions from an ungated HEMT using full-wave hydrodynamic model, IEEE Trans. Electron Devices **63**, 990 (2016).

[27] M. Nafari, G. R. Aizin, and J. M. Jornet, Plasmonic HEMT terahertz transmitter based on the Dyakonov-Shur instability: Performance analysis and impact of nonideal boundaries, Phys. Rev. Appl. **10**, 064025 (2018).

[28] V. Ryzhii, T. Otsuji, and M. Shur, Graphene based plasma-wave devices for terahertz applications, Appl. Phys. Lett. **116**, 140501 (2020).

[29] M. Shur, G. Aizin, T. Otsuji, and V. Ryzhii, Plasmonic field-effect transistors (TeraFETs) for 6G communications, Sensors **21**, 7907 (2021).

[30] M. Dyakonov and M. Shur, Current instability and plasma waves generation in ungated two-dimensional electron layers, Appl. Phys. Lett. **87**, 111501 (2005).

[31] C. B. Mendl and A. Lucas, Dyakonov-Shur instability across the ballistic-to-hydrodynamic crossover, Appl. Phys. Lett. **112**, 124101 (2018).

[32] D. Svintsov, V. Vyurkov, V. Ryzhii, and T. Otsuji, Hydrodynamic electron transport and nonlinear waves in graphene, Phys. Rev. B **88**, 245444 (2013).

[33] W. Shockley, A unipolar "field-effect" transistor, Proc. IRE **40**, 1365 (1952).

[34] G. Birkhoff and S. Mac Lane, *A Survey of Modern Algebra*, 4th ed. (Macmillan Publishing, New York, 1977), pp. 102, 119, 120.

[35] M. Abramowitz, Elementary analytical methods, in *Handbook of Mathematical Functions with Formulas, Graphs, and Mathematical Tables*, edited by I. A. Stegun and M. Abramowitz (Dover, New York, 1972), p. 17.

[36] J. Bezanson, A. Edelman, S. Karpinski, and V. B. Shah, Julia: A fresh approach to numerical computing, SIAM Rev. **59**, 65 (2017).